Title
Rapid and Ultrasensitive Hydrogen Sensing: From Single Nanowires to Carbon Nanotubes

Author
Li, Xiaowei

Publication Date
2016

Peer reviewed|Thesis/dissertation

UNIVERSITY OF CALIFORNIA,
IRVINE

Rapid and Ultrasensitive Hydrogen Sensing: From Single Nanowires to Carbon Nanotubes

DISSERTATION

submitted in partial satisfaction of the requirements
for the degree of

DOCTOR OF PHILOSOPHY

in Materials and Manufacturing Technology

by

Xiaowei Li

Dissertation Committee:
Professor Reginald M. Penner, Chair
Professor James C. Earthman
Professor Daniel R. Mumm

2016

DEDICATION

To Rachel and Leo, my angels, love and life.
To my beloved family and all my dear friends,
for your tremendous support through my whole PhD.
I would like to express my sincere appreciation to my advisor Dr. Reginald M. Penner,
for his patience, enthusiam, and immense knowledge,
for understanding, encouraging and mentoring me,
guiding and supporting my research, my exploration in nano-world.

TABLE OF CONTENTS

LIST OF FIGURES

LIST OF TABLES

ACKNOWLEDGMENTS

I would like to thank my PhD thesis advisor, Professor Reginald M. Penner. I have spent my whole PhD in Reg's research group, and I really enjoy these years for which I have worked with him. Reg has been guiding me in exploring the world of nanotechnology as a wise mentor, an experienced partner and a great friend. I have learned a lot from him, particularly his impressive enthusiasm and scientific spirits of conducting research. Under his guidance, I have broadened my perspective to nanoscale chemical sensors and enhanced my skill sets with electrochemistry, nanofabrication and electron microscopy. He has been very supportive to me for providing suggestive opinions, showing where the cutting-edge is, introducing the research pioneers and moreover, my idea on controllable patterning ultralong carbon nanotube ropes. We had a hard time at the first beginning, since it's the first carbon nanotubes research project we've ever had and I barely have any experimental experience for dealing with this precious materials. From communicating with Reg, I've learned the essences for making breakthrough in research To be creative, careful and persistent. Without his trust and guidance, I cannot imagine that I have been reaching out so far until now to get my PhD.

I would like to thank my committee members, Professor James C Earthman and Professor Daniel R. Mumm, for serving in my qualification exam and also my PhD defense. Thank you all for the courses you taught in the graduate school and your advices towards my PhD thesis. Meanwhile, I wish to thank Division of Chemistry of National Science Foundation for financially supporting our research projects with award number CHE-1306928. I also would like to thank Professor Eric Potma, Dr. Junghoon Jahng for the valuable discussion and collaboration, and Dr. Jian-Guo Zheng, Dr. Qi-Yin Lin, Dr. Matthew Sullivan and Dr. Ming-Je Sung for your tremendous help on my electron microscopy experiments, all electron microscopy images included in this thesis were acquired in the Laboratory for Electron and X-ray Instrumentation (LEXI) at University of California, Irvine.

In the end, I wish to highly appreciate my classmates and dear friends for your long time support, and my lab colleagues in Penner group for the valuable discussions on my research.

CURRICULUM VITAE

Xiaowei Li

EDUCATION

Doctor of Philosophy in Engineering — **Dec. 2016**
University of California, Irvine — *Irvine, CA*

Advisor: Dr. Reginald M. Penner

Master of Science in Engineering — **Jun. 2012**
University of California, Irvine — *Irvine, CA*

Bachelor of Science in Physics — **Jun. 2009**
Nankai University — *Tianjin, China*

RESEARCH EXPERIENCE

Graduate Research Assistant in Reg Penner Group — **Jul. 2011 – Dec. 2016**
University of California, Irvine — *Irvine, California*

Graduate Research Assistant in Yufang Wang Group — **Sep. 2008 – Jun. 2009**
Nankai University — *Tianjin, China*

TEACHING EXPERIENCE

Teaching Assistant of General Chemistry Lab — **Mar. 2016 – Jun. 2016**
University of California, Irvine — *Irvine, CA*

REFEREED JOURNAL PUBLICATIONS

11. **X. Li**, R. M. Penner*, Palladium Nanoparticle-Decorated Carbon Nanotube Ropes for Rapid, Sensitive H_2 Detection, *In preparation.*

10. G. T. Chandran, **X. Li**, A. Ogata, R. M. Penner*, Review on Nanostructured Materials, *Anal. Chem.*, *submitted.*

9. S. Qiao, Q. Xu, R. K. Dutta, M. Le Thai, X. Li, R. M. Penner*, Electrodeposited, Transverse Nanowire Electroluminescent Junctions, *ACS Nano*, 10 (2016) 8233.

8. M. Le Thai, G. T. Chandran, R. K. Dutta, **X. Li**, and R. M. Penner*, 100k Cycles and Beyond: Extraordinary Cycle Stability for MnO_2 Nanowires Imparted by a Gel Electrolyte, *ACS Energy Lett.*, 1 (2016) 57.

7. J. Jahng, F. T. Ladani, R. M. Khan, **X. Li**, E. S. Lee, and E. O. Potma*, Visualizing Surface Plasmon Polaritons by Their Gradient Force, *Opt. Lett.*, 40 (2015) 5058.

6. Q. Xu, S. Qiao, R. K. Dutta, M. Le Thai, **X. Li**, C. Eggers, G. T. Chandran, Z. Wu, and R. M. Penner*, A 30 μm Coaxial Nanowire Photoconductor Enabling Orthogonal Carrier Collection, *Nano Lett.*, 15 (2015) 5861.

5. **X. Li**, Y. Liu, J. C. Hemminger and R. M. Penner*, Catalytically Activated Palladium@Platinum Nanowires for Accelerated Hydrogen Gas Detection, *ACS Nano*, 9 (2015) 3215 .

4. J. Jahng, J. Brocious, D. A. Fishman, F. Huang, **X. Li**, V. A. Tamma, H. K. Wickramasinghe*, and E. O. Potma*, Gradient and Scattering Forces in Photoinduced Force Microscopy, *Physical Review B*, 90 (2014) 155417.

3. W. Yan, M. Le Thai, R. K. Dutta, **X. Li**, W. Xing, and R. M. Penner*, A Lithographically Patterned Capacitor With Horizontal Nanowires of Length 2.5 mm, *ACS App. Mater. & Interfaces*, 6 (2014) 5018.

2. F. Sun, **X. Li**, Fatigue Performance Study on 2A12CZ of Laser Cladding Al-Y Powder, *J. of Qingdao Univ. (Nat. Sci. Edition)* 2 (2008) 7.

1. **X. Li**, W. Xu, Trusted Computing Platform Research of Designing Safe Chip, *Dual Use Technologies & Products* 8 (2008) 019.

SELECTED PRESENTATIONS

Lithographically Patterned Single-Walled Carbon Nanotubes Electrophoretic Deposition **2015**
MRS Fall Meeting & Exhibit, Boston, MA, USA

Catalytically Activated Palladium@Platinum Nanowires for Accelerated Hydrogen Gas Detection **2015**
MRS Fall Meeting & Exhibit, Boston, MA, USA

Catalytically Enhanced Palladium Nanowire Sensing of Hydrogen **2015**
ACS National Meeting, Denver, CO, USA

ABSTRACT OF THE DISSERTATION

Rapid and Ultrasensitive Hydrogen Sensing: From Single Nanowires to Carbon Nanotubes

By

Xiaowei Li

Doctor of Philosophy in Materials and Manufacturing Technology

University of California, Irvine, 2016

Professor Reginald M. Penner, Chair

Nanoscale devices take many advantages, including low power consumption for energy saving, highly miniaturized structures for portable equipment and tiny amount of materials needed for manufacturing purposes, particularly considering rare metals. Nano-devices have exhibited significant potentials for wide industrial applications, for example, chemical and biological sensing, nano-electronics, environment and health monitoring etc. In this dissertation, two types of H_2 sensors are discussed, they are based on single metal nanowires and metal nanoparticles-decorated carbon nanotube (CNT) ropes respectively.

Single nanowire H_2 sensors are fabricated by applying the methods of lithographically patterned nanowire electrodepositon (LPNE). Single palladium (Pd) nanowires with the dimension of 40 nm (height) $\times$ 100 nm (width) $\times$ 50 μm (length) are electrodeposited within LPNE templates and electrically isolated by metal contacts. Then platinum (Pt) layers are electrodeposited onto single Pd nanowires (Pd@Pt nanowires) to catalytically enhance the H_2 sensing performance. The Pt layer coverage thickness is altered as average 0.1 monolayer (ML), 1 ML and 10 ML. For each coverage, the Pd@Pt nanowire sensors are evaluated at five different working temperatures, Pd@Pt sensors exhibited lowest detection at 500 ppm H_2 exposure. Both response and recovery behaviors of Pd@Pt sensors are accelerated at

higher temperature, yet the drawback is deterioration of sensitivity and detection limit.

A type of more advanced H_2 sensors based on semiconducting CNT ropes are developed, in order to enhance the H_2 sensing performance for rapid response/ recovery and wider detection range. CNT ropes deposition are achieved by applying processes of dielectrophoresis in aqueous solution containing suspended CNTs. Single CNT ropes are electrical isolated at the length of 50 μm, and employed as the electrode for electrodepositing Pd nanoparticles of four coulombic loadings. Bare CNT ropes show no response to H_2/ air exposures, however the sensitivity to H_2 is very strongly enhanced. Pd–CNT sensors are capable of detecting H_2 mixture in a very wide range between 10 ppm to 4 vol% at room temperature. The influence of Pd nanoparticle diameter to H_2 sensing is also evaluated.

Chapter 1

Introduction

1.1 Introduction to Hydrogen Sensors

H_2 is the lightest gas, it is odorless, colorless and tasteless at ambient temperature and standard pressure, human being cannot sense the existence of H_2 by organs. H_2 gas is highly flammable and can be explosive in air at a very wide concentration range from 4 vol% to 75 vol% by generating a lot of heat[4], the enthalpy of combustion is -286 kJ/ mol. H_2 has been widely used in many industrial applications, it can be used as additives in petroleum and chemical industries, for processing fossil and producing NH_3 etc. H_2 is also commonly used as rotor coolant in electrical generators at power plants due to it's of the highest thermal conductivity. Moreover, H_2 is a clean energy source for commercialized electric vehicles loaded with fuel cell engines producing H_2O as only by-product. After all, utilization of H_2 can be dangerous, and the most critical risk factor is H_2 leakage. The rapid, sensitive

detection of leaked hydrogen gas in air remains technologically challenging.[1, 54, 3, 21, 2] The U.S. Department of Energy has defined performance metrics including the response and recovery speed, sensitivity, limit-of-detection (LOD_{H_2}), and the cost (< \$40/unit) as well as other attributes (Table 2.1).[48] The cost requirement constrains the technologies that can be explored in these sensors.

1.2 Nanowire Hydrogen Gas Sensors

One attractive option is palladium and palladium alloy resistors, first demonstrated by Hughes and Schubert in 1992.[22] When these DOE metrics were published in 2009[48, 39], no H_2 sensor was capable of achieving all of them and this remains the case today, but nanoscience has enabled considerable progress with resistor-based sensors for H_2. Amongst the most challenging of the DOE metrics are the response and recovery times: A response time for H_2 exposure of <1s at 4% H_2 and <60s at 1% are required in an air ambient, as is a recovery time of less than 60s, independent of H_2 concentration. Single palladium (Pd) nanowires,[49, 78, 77, 75, 76, 74, 12, 67, 66] films of Pd nanoparticles,[73, 80, 26] Pd nanowire networks,[80, 81] and Pd structures with engineered nanogaps[29, 30] have accelerated sensor response and recovery speed but in most cases, these advances have been demonstrated for H_2 sensing in a background of N_2, not air.[12, 66, 29, 34, 30, 73, 78, 75, 77, 80, 81].

In our group, there is long period interests in developing H_2 gas sensors, the research history spans over 15 years since 2001. Previous lab members have developed Pd mesowire arrays [12] as the first generation H_2 sensors, this type of sensors is of fast H_2 detection capability, but to take the disadvantages of imprecise fabrication and unsatisfied detection limit. Since 2009, single Pd and Pt nanowires as the advanced version of H_2 sensors[75, 78, 74] have been

created and developed. Thank to the unique method of LPNE, the dimension and geometry of these single nanowire sensors can be precisely controlled, lowest detection limit has been extended to 1 ppm H_2 mixed in N_2 and 500 ppm for H_2 balanced in air. In addition, the fabrication processes are standardized and yield is greatly improved if compared to the Pd mesowire arrays.

I have contributed my efforts to develop Platinum (Pt)-modified palladium (Pd) nanowires (or Pd@Pt nanowires) with controlled Pt coverages as the succeeded version[39]. These Pd@Pt nanowires are used as resistive gas sensors for the detection of hydrogen gas in air, and the influence of the Pt surface layer is assessed. Pd nanowires with dimensions of 40 nm(h) $\times$ 100 nm(w) $\times$ 50 μm(l) are first prepared using lithographically-patterned nanowire electrodeposition (LPNE). A thin Pt surface layer is electrodeposited conformally onto a Pd nanowire at coverages, θ_{Pt}, of 0.10 monolayer (ML), 1.0 ML, and 10 ML. X-ray photoelectron spectroscopy coupled with scanning electron microscopy and electrochemical measurements are consistent with a layer-by-layer deposition mode for Pt on the Pd nanowire surface. The resistance of a single Pd@Pt nanowire is measured during the exposure of these nanowires to pulses of hydrogen gas in air at concentrations ranging from 0.05 to 5.0 vol%. Both Pd nanowires and Pd@Pt nanowires show a prompt, reversible increase in resistance upon exposure to H_2 in air, caused by the conversion of Pd to more resistive PdH_x. Relative to a pure Pd nanowire, the addition of 1.0 monolayer (ML) of Pt to the Pd surface alters the H_2 detection properties of Pd@Pt nanowires in two ways: First, the amplitude of the relative resistance change, $\Delta R/R_0$, measured at each H_2 concentration is reduced at low temperatures (T = 294K and 303K), and enhanced at higher temperatures (T = 316, 344, and 376 K). Second, response and recovery rates are both faster at all temperatures in this range, and for all H_2 concentrations. For higher θ_{Pt} = 10 MLs, sensitivity to H_2 is dramatically reduced. For lower θ_{Pt} = 0.1 ML, no significant influence on sensitivity or the speed of response/recovery is observed.

1.3 Pd–Carbon Nanotube Hydrogen Gas Sensors

In the third chapter, palladium (Pd) nanoparticle-decorated carbon nanotube (CNT) ropes (or Pd-CNT ropes) are discussed as the sensing element for hydrogen gas (H_2) sensors. Pd-CNT rope sensors enable the detection of H_2 with response/recovery times in air that are faster than observed for single palladium (Pd) nanowires, while also enabling a much wider dynamic range, encompassing [H_2] from 10 ppm to 4%. Pd-CNT rope sensors are prepared by the dielectrophoretic deposition of a single semiconducting CNT rope followed by the electrodeposition of Pd nanoparticles with mean diameters ranging from 4.5 ($\pm$ 1) nm to 5.8 ($\pm$ 3) nm. The diminutive mean diameter and the high degree of diameter monodispersity for the deposited Pd nanoparticles are distinguishing features of the Pd-CNT rope sensors described here, relative to prior work. Earlier, the deposition of palladium (Pd) particles on carbon nanotubes (CNTs) has been used to prepare H_2 sensors, but response and recovery times were often slow and the dynamic range limited. We attribute accelerated response/recovery and greater H_2 sensitivity to the reduced nanoparticle diameter, and greater diameter uniformity, enabled using electrodeposited Pd nanoparticles.

Chapter 2

Catalytically Activated Palladium@Platinum Nanowires for Accelerated Hydrogen Gas Detection

2.1 Introduction

Hydrogen safety sensors must function in air, a much more challenging ambient for H_2 sensing than N_2. For example, we[78, 75] reported that single Pd nanowires operating at 300°C in N_2 showed a LOD_{H_2} of 2 ppm and response/recovery times of 40s/300s for exposure to 0.10% H_2. But for a similar Pd nanowire operating in dry air,[78, 75] LOD_{H_2} was increased to 100 ppm, and response/recovery times were increased to 400s/1000s. The deleterious influence of air can be rationalized as follows: In the an N_2 ambient, dihydrogen physisorbs onto the

Pd surface, dissociates, and chemisorbs, forming Pd-H (Fig 1):

$$H_2(g) \longrightarrow H_2(ads) \tag{2.1}$$

$$Pd + \frac{1}{2}H_2(ads) \longrightarrow Pd\text{-}H \tag{2.2}$$

The electrical resistivity of $PdH_{0.7}$ is almost a factor of two higher than that of palladium,[38] allowing the presence of H_2 to be detected as an increase in the resistance of the Pd resistor. Air increases the LOD_{H_2} because the presence of oxygen[15] enables catalytic water formation at the Pd surface, thereby reducing the steady-state surface coverage of chemisorbed hydrogen available to be absorbed into the bulk of the PdH_x (reaction (2) above)[14, 50](Fig 1)

$$Pd\text{-}O + \frac{3}{2}H_2(ads) \longrightarrow Pd\text{-}H + H_2O(ads) \tag{2.3}$$

$$H_2O(ads) \longrightarrow H_2O(g) \tag{2.4}$$

Chemisorbed oxygen (reaction 3) also blocks Pd adsorption sites, impeding hydrogen adsorption and extending the time required for equilibration of hydrogen in the gas phase with the PdH_x, retarding both response and recovery. The strong influence of oxygen on the sensing behavior of Pd nanowires shows that surface chemistry is a critical factor in determining the performance of resistance-based hydrogen gas sensors.

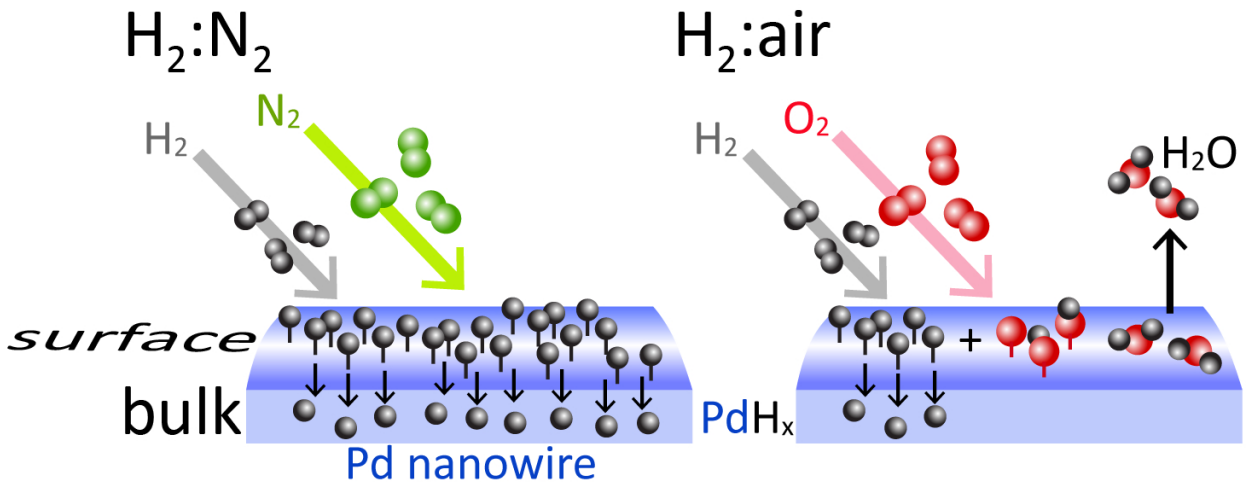

Figure 2.1: Schematic representation of the influence of oxygen in air on the response of a Pd nanowire to H_2. The sensitivity of the nanowire resistance to H_2 and the speed of the response and recovery of the resistance are reduced in air as compared with N_2.

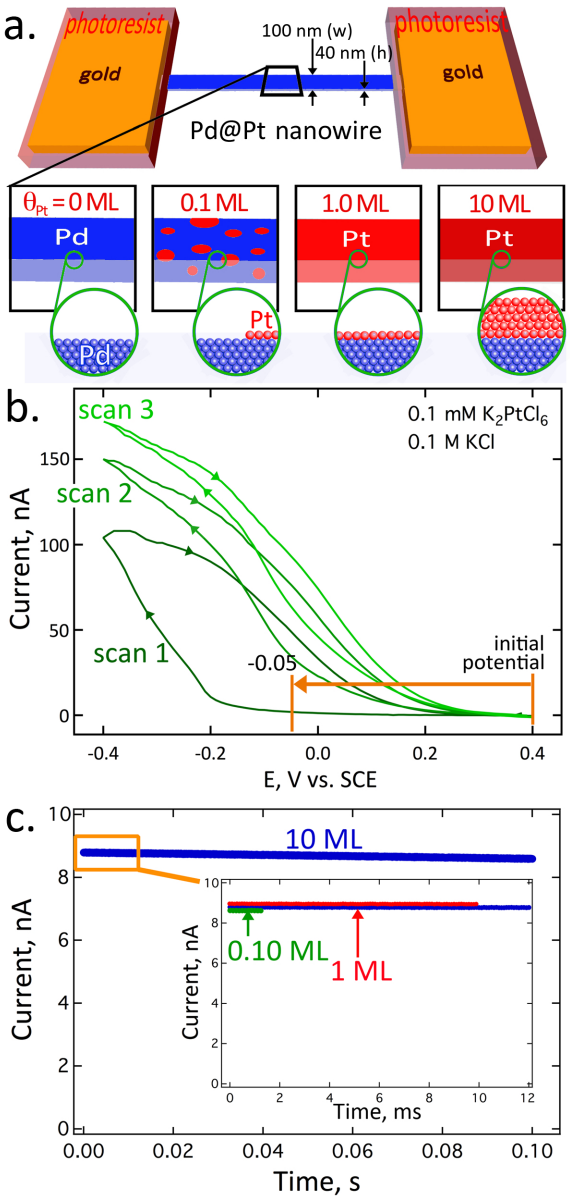

Figure 2.2: Electrodeposition of Pt on a Pd nanowire. a) Pd@Pt nanowires were prepared by electrodepositing controlled quantities of Pt, based upon deposition charge, onto a single Pd nanowire prepared using LPNE, as shown schematically here. b) Cyclic voltammetry of a Pd nanowire in aq. 0.1 mM K_2PtCl_6, 0.1 M KCl. Platinum metal was electrodeposited from aqueous KCl solution at -0.05 V vs. saturated calomel electrode (SCE.) Under these deposition conditions, layer-by-layer deposition of Pt is expected, as indicated schematically in (a). c) Current *versus* time transients showing a constant Pt deposition current as a function of time, as expected for a kinetically-controlled layer-by-layer deposition mechanism. The deposition charge associated with the electrodeposition of a Pt monolayer from a solution of $PtCl_6^{2-}$ is 832 μQ/cm^2.

One tactic for accelerating response and recovery in both air and N_2 is to heat a Pd nanowire.[77] At a Pd nanowire, both response to H_2 and recovery from it are strongly thermally activated.[77] But even after optimization of the elevated nanowire temperature at 428K, the resulting performance (Table 2) does not meet the requirements summarized in Table 1. An obvious place to look for an additional improvement is the nanowire surface chemical composition.

The formation of a Pt shell on a Pd nanowire has the potential to favorably alter the surface chemistry of a Pd nanowire. Johannson *et al.*[25] have shown that in dry air at $T = 100°C$, Pt is a better catalyst than Pd for reaction (3). Pt is also a superior catalyst for reaction (2) which is the rate-limiting reaction for sensor response in N_2.[77] We[74] recently prepared platinum nanowires and evaluated their performance as hydrogen sensors. To our surprise, we found dramatic increases in response speed for sensors based on Pt nanowires, but even slower sensor recovery as compared with Pd nanowires of the same size.[74] For example, for a Pt nanowire operating in air at 550K, the response time was decreased by a factor of 100 at 1.0% H_2 while under identical conditions, the recovery time was slower than for a Pd nanowire of identical size by a factor of 14 (1000s *versus* 70s).[74]

Here, we assess the influence of ultra-thin Pt layers, corresponding to a Pt coverage, θ_{Pt}, of 0.10 ML to 10 ML, on the hydrogen sensing performance of a Pd nanowire in air. Pt layers were prepared by electrodeposition under conditions that promote a layer-by-layer deposition mode for platinum onto the Pd nanowire surface. We find that the Pt layer accelerates both the response and recovery to hydrogen in air. Importantly, Pt increases the limit-of-detection for hydrogen (LOD_{H_2}) at room temperature, but extends it to lower values at elevated temperatures of 376K enabling simultaneous acceleration of response/recovery with minimum degradation of the sensitivity to H_2. The net effect is that for an optimum Pt coverage of $\theta_{Pt} = 1.0$ ML, the H_2 sensing performance in air of a Pd@Pt nanowire operating at $T = 376$K is significantly improved relative to pure Pd nanowire - the current state-of-

the-art - operating anywhere in the temperature range from 294K to 376K.

2.2 Results and Discussion

2.2.1 Preparation and Characterization of Platinum-Modified Palladium Nanowires

Palladium nanowires with lateral dimensions of 40 nm (h) × 100 nm (w) and lengths of more than 100 μm were prepared using Lithographically Patterned Nanowire Electrodeposition (LPNE) as previously described.[72, 78, 77, 75, 76] Gold electrical contacts were then patterned using photolithography, metal evaporation and liftoff to electrically address a 50 μm section of this nanowire (Fig 2a). These contacts were covered with a photoresist layer to insulate them from contact with the platinum plating solution, and the dilute, aqueous H_2SO_4 electrolyte used for electrochemical nanowire characterization.

Surface-limited redox replacement (SLRR) is an elegant method for electrodepositing monolayer quantities of a noble metal on the surface of another noble metal.[16, 13, 47] SLRR is a two step process involving the under-potential deposition (UPD) of a monolayer of a non-noble metal (e.g., Cu) onto a noble metal electrode (e.g., Pd) followed by galvanic replacement$^{e.g.}$[62, 5, 65] of the Cu by a noble metal such as Pt. In contrast, for the particular system of interest here (Pt on Pd), instead of using an SLRR method we have used a single over potential (OPD) step to grow Pt in a layer-by-layer fashion on the palladium nanowire. This was accomplished by stepping the potential of the nanowire from +0.40V to -0.050V vs. saturated calomel reference electrode (SCE) in a solution containing 0.1 mM K_2PtCl_6 in 0.10 M HCl. As shown in the cyclic voltammogram in Fig 2b, -0.050V is well positive of the potential where a rapid increase in the reduction current signals the onset of

nucleation of three-dimensional Pt islands on the Pd surface ($\sim$ -0.20 V). At potentials positive of this onset, our data indicate that the electrodeposition of Pt occurs by a layer-by-layer process as detailed below.

A layer-by-layer, or Frank–Van der Merwe,[79] growth mechanism for Pt deposition onto the Pd nanowire is supported by three experimental observations: First, the deposition current is constant as a function of time (Fig 2c). This behavior has also been seen previously for Pt on Pd electrodeposition [19] as well as for other metal-on-metal deposition systems at low overpotentials.[46, 51] At higher overpotentials (more negative deposition potentials), layer-by-layer growth is replaced by the growth of three-dimensional metal nuclei.[46, 51, 19] This Volmer-Webber growth mode[79] is characterized by a peak shaped current *versus* time response that is diagnostic of either instantaneous or progressive nucleation of three-dimensional nuclei.[20, 57, 58] Second, no three-dimensional nuclei are observed in scanning electron microscope (SEM) images of these nanowires acquired after Pt deposition, for any of the Pt coverages examined here, at any magnification (e.g., Fig 3e). Such particles should be observed if the three-dimensional growth of Pt on the Pd surface is occurring. Moreover, EDX elemental maps (Fig 3g) show that the deposited Pt is uniformly distributed on the surface of a Pd@Pt nanowire with $\theta_{Pt} = 10$ MLs, as expected for the deposition of conformal Pt layers. Third, X-ray photoelectron spectroscopy (XPS) analysis for Pd and Pt (Fig 4) shows a strong, linear decrease in the Pd photoelectron signal with the deposition of 10 and 20 MLs of Pt onto clean Pd nanowire surfaces. This attenuation of the Pd XPS signal is only expected if the Pd surface is covered by a conformal Pt layer. In contrast, a weaker, nonlinear attenuation of the Pd XPS signal is expected with Pt deposition if prompt, three-dimensional nucleation and growth of Pt is occurring.

It is important to appreciate that the alloying of the electrodeposited Pt with Pd is possible in principle. Both Pd and Pt are detected by XPS for $\theta_{Pt} = 20$ML (Fig 4), but the abruptness of the Pd/Pt interface can not be discerned from these data.

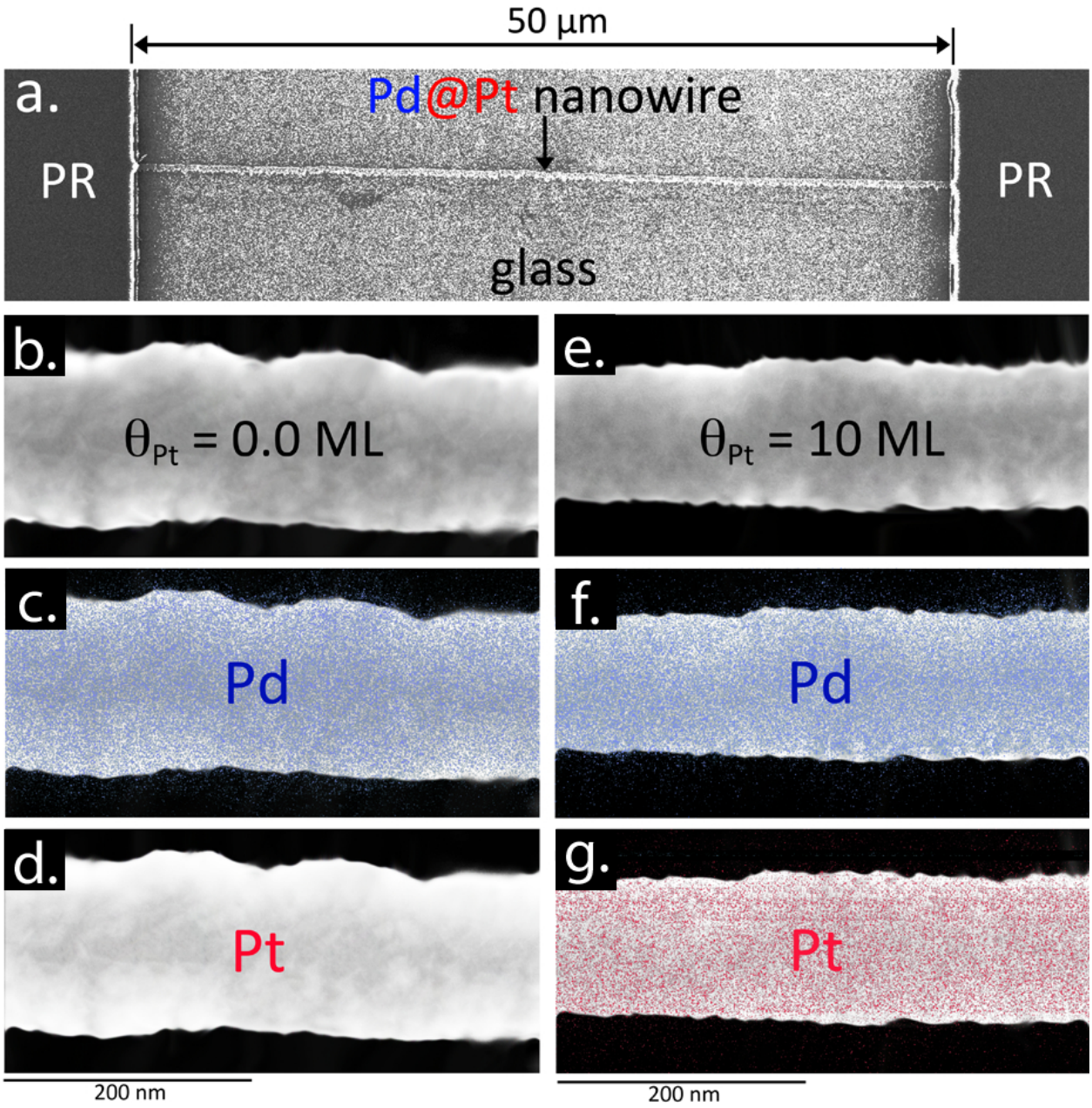

Figure 2.3: SEM and EDX analysis of Pd and Pd@Pt (10 ML) nanowires. a) A low magnification SEM image of a single nanowire H_2 sensor showing the photoresist(PR)-covered gold contacts. b-d) Pd nanowire with no deposited Pt. e-g) Pd@Pt nanowire with $\theta_{Pt} = 10$ MLs. Shown are: (b,e) secondary electron images, (c,f) EDX elemental map for Pd superimposed on the image of (a), (d,g) EDX elemental map for Pt.

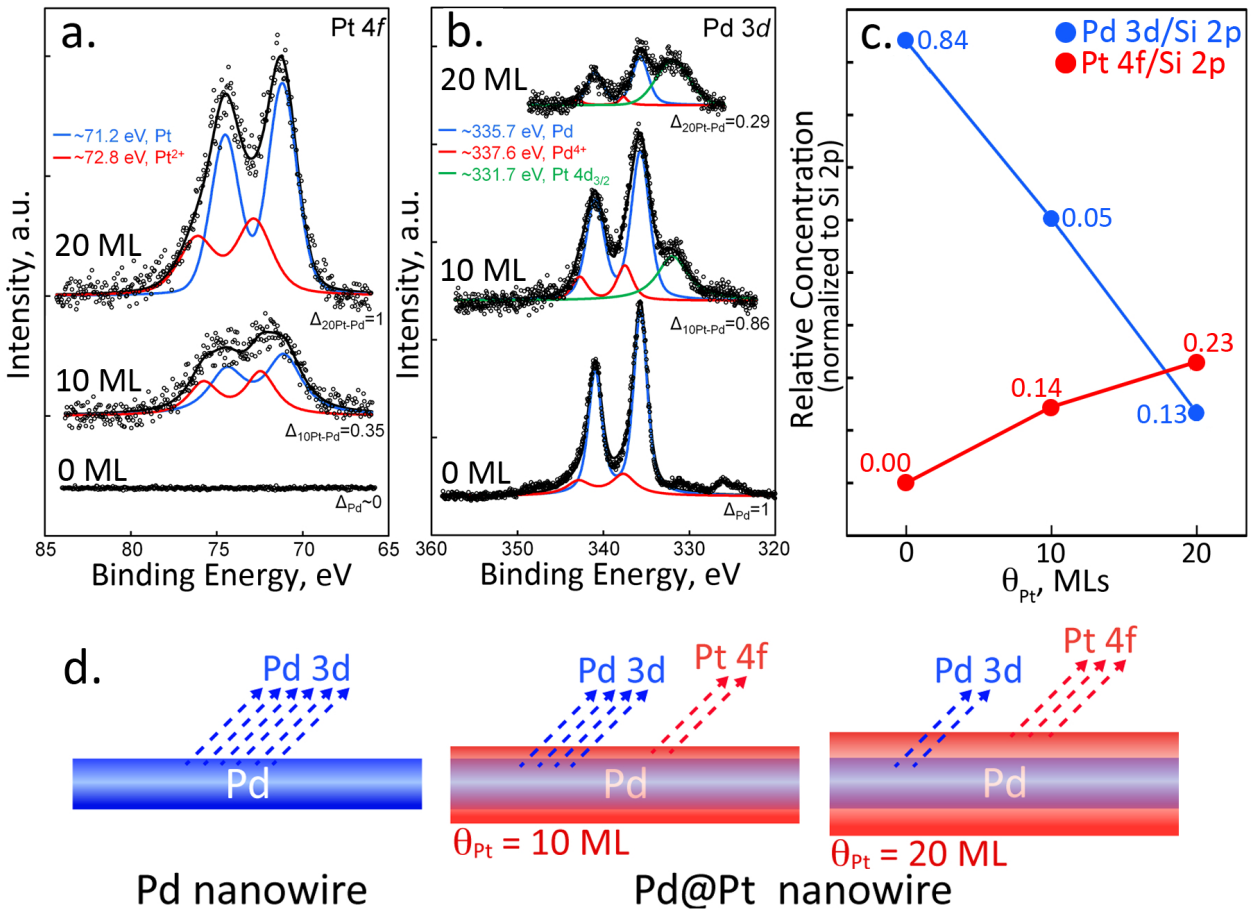

Figure 2.4: XPS analysis of Pd@Pt nanowires. a) Pt 4f spectra at θ_{Pt} = 0 ML, 10 ML, and 20ML showing buildup of intensity with coverage. b) Pd 3d XPS spectra ($3d_{3/2}$ at 340 eV and $3d_{5/2}$ at 335 eV) at the same θ_{Pt} values as in (a) showing strong attenuation of the Pd 3d photoelectrons with the deposition of Pt. c) Integrated intensity *versus* θ_{Pt} for Pt 4f (red trace) and Pd 3d (blue trace) photoelectrons showing linear increase and decrease, respectively, of the photoelectron intensity.

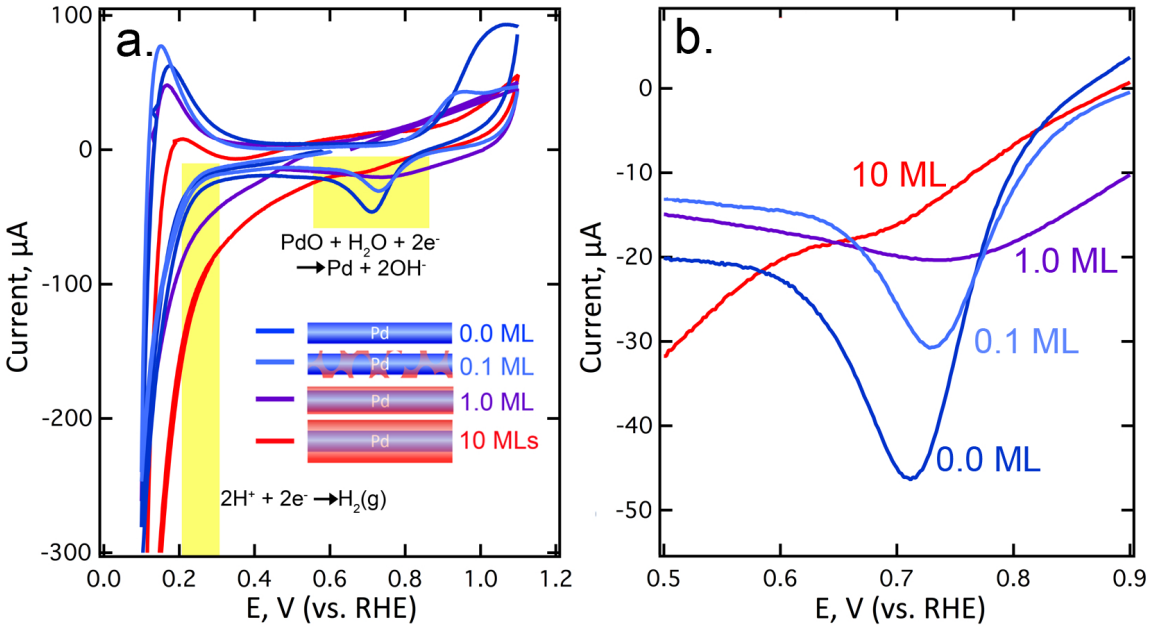

Figure 2.5: Voltammetry of arrays of Pd nanowires and Pd@Pt nanowires. a) Cyclic voltammograms at 20 mV/s in aq. 0.050 M H_2SO_2 showing oxide formation (+1.0 V vs. RHE, reversible hydrogen electrode), oxide reduction (0.7 - 0.8 V) and hydrogen evolution at (-0.20 V). Hydrogen evolution currents at -0.20 V progressively increase in the order $\theta_{Pt} = 0.0 \approx 0.1 < 1.0 < 10$ MLs, qualitatively as expected.[17] b) Palladium oxide reduction region of the CVs shown in (a) highlighting the increased reduction peak currents in the order: $\theta_{Pt} = 0.0 > 0.1 > 1.0 > 10$ MLs. A positive shift in the peak potential for oxide reduction with increasing Pt coverage is also observed, as previously documented.[18, 17, 52]

Finally, with increasing θ_{Pt}, the cyclic voltammetry of Pd@Pt nanowires in aqueous 0.050 M H_2SO_4 shows the emergent characteristics of a surface Pt layer (Fig 5a). Specifically, the peak current for the oxide reduction (≈0.75 V vs. RHE) decreases as Pt is deposited on the Pd surface, and the peak potential of this oxide peak shifts positive as previously reported (Fig 5b).[18, 17, 52] The catalytic activity of the surface for proton reduction at ≈0.20 V (Fig 5a) also increases with θ_{Pt}, in agreement with previously observations.[17] The smooth evolution of the cyclic voltammetry of these nanowires with increasing θ_{Pt} does not prove that Pt is deposited in a layer-by-layer fashion, but it does indicate that the electrocatalytic properties of the nanowires are modified monotonically with increasing Pt coverage, even for the deposition of extremely small amounts of Pt. In the following, we exploit the modified catalytic properties of Pd@Pt nanowires for H_2 gas detection in air.

2.2.2 Detection of Hydrogen in Air

The temperature-dependent properties of Pd and Pd@Pt nanowires for the detection of H_2 in air were probed over the temperature range from 294K to 376K (Fig 6). Elevated nanowire temperatures were achieved by controlled Joule-heating of the nanowire. Joule-heating was effected by increasing the applied voltage to the nanowire, thereby increasing the current, i, and causing the dissipation of the resulting i^2R as heat. The temperature of the nanowire was determined with ±1K accuracy from its electrical resistance in the absence of hydrogen. Calibration of the nanowire resistance with temperature is described in the experimental section. The resistance *versus* time performance of a 40 nm × 100 nm Pd nanowire for detecting H_2 in air, for example, is shown in Fig 6a. The sensitivity of this nanowire is excellent at 294K but response and recovery times are much too slow relative to DOE metrics outlined in Table 1. Heating the nanowire accelerates both response and recovery, at the cost of some loss of sensitivity (Fig 6a), but even at 344K, this sensor is not fast enough. The

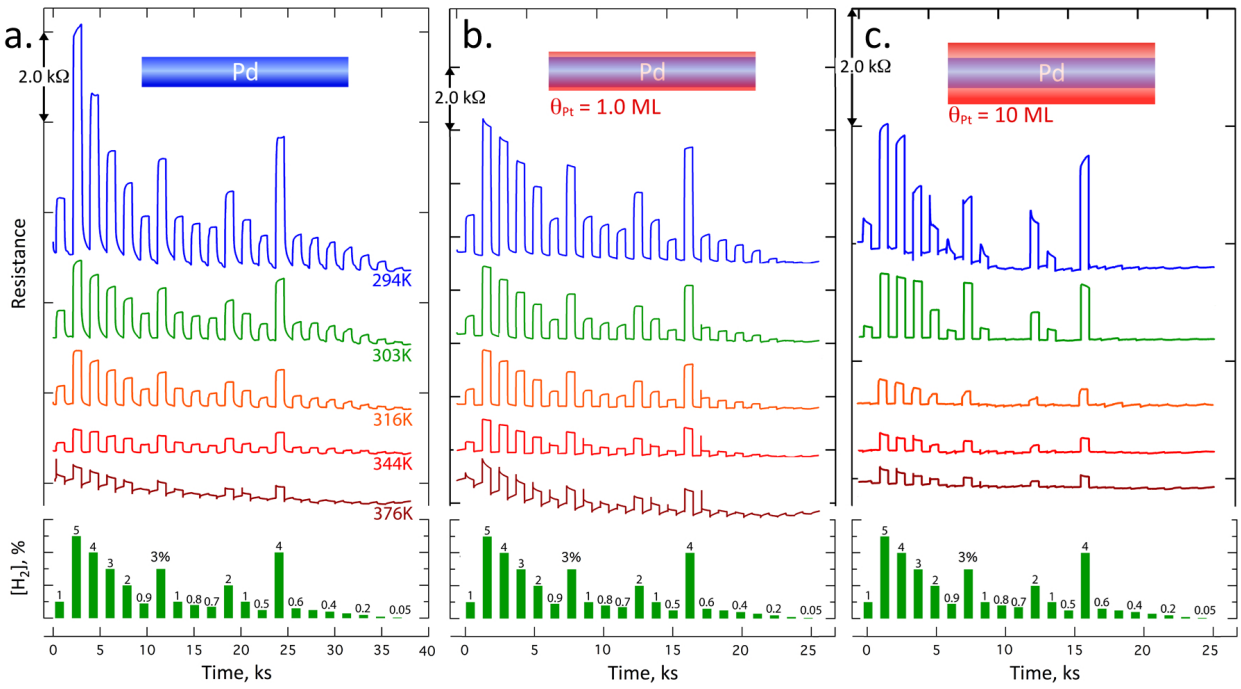

Figure 2.6: Raw H_2 sensing responses for three nanowires at five temperatures from 294K to 376K: a) A Pd nanowire with dimensions of 40 nm(h) × 100 nm(w) × 50 μm(l). b) A Pd@Pt nanowire with θ_{Pt} = 1.0 ML., c) A Pd@Pt nanowire with θ_{Pt} = 10 ML. Note that the time scale in (b) and (c) is compressed by 30% relative to (a).

performance of single Pd nanowires for detecting H_2 in N_2[78, 77, 75, 76, 23, 24, 49, 80, 81] and in air,[77, 75] is state-of-the-art, and the performance seen in Fig. 6a is consistent with this prior published work for Pd nanowire H_2 sensors operating in air.[77, 75]

Relative to a pure Pd nanowire, the addition of a Pt layer alters the H_2 detection properties of Pd@Pt nanowires in two ways (Fig 6b,c): First, the amplitude of the relative resistance change, $\Delta R/R_0$ (where R_0 is the initial resistance of the nanowire), measured at each H_2 concentration is reduced at low temperatures (T = 294K and 303K), whereas $\Delta R/R_0$ at higher temperatures (T = 316K, 344K, and 376K) is approximately the same as for pure Pd nanowires (Fig 7). Second, response and recovery rates are accelerated at all temperatures in this range, and for all H_2 concentrations. (Figs 8,9). We discuss both of these effects below.

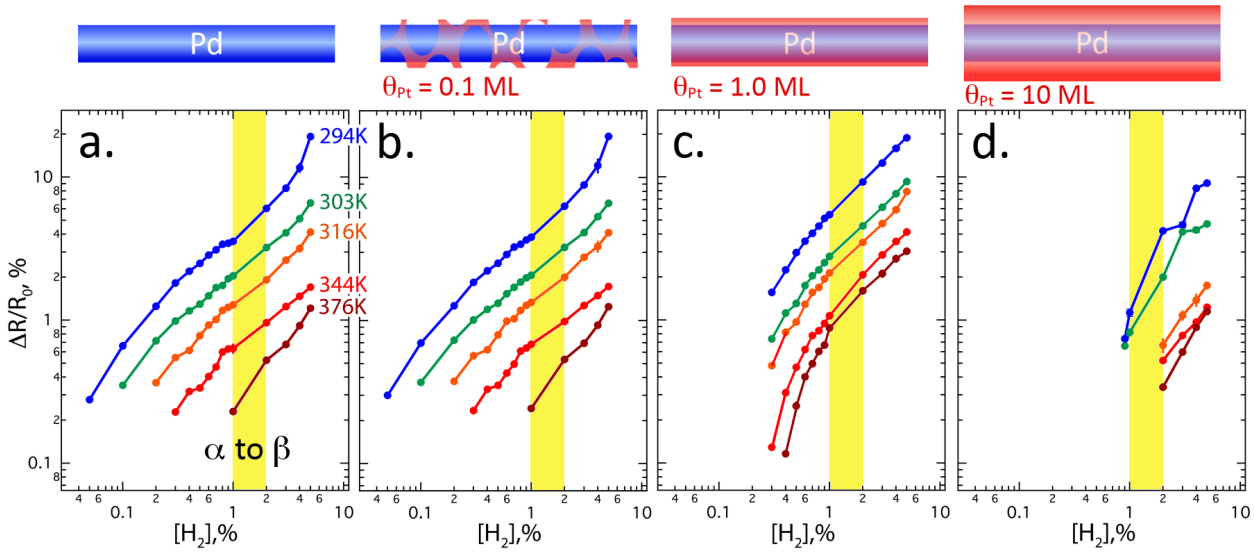

Figure 2.7: Calibration plots as a function of temperature. Plotted are the normalized resistance change, $\Delta R/R_0$, *versus* [H_2] for: a) a pure Pd nanowire, $\theta_{Pt} = 0$ ML, b) a Pd@Pt nanowire with $\theta_{Pt} = 0.1$ ML, c) a Pd@Pt nanowire with $\theta_{Pt} = 1.0$ ML, and, d) a Pd@Pt nanowire with $\theta_{Pt} = 10$ ML. The yellow region from 1-2% [H_2] coincides with the α-to-β phase transition of PdH_x.

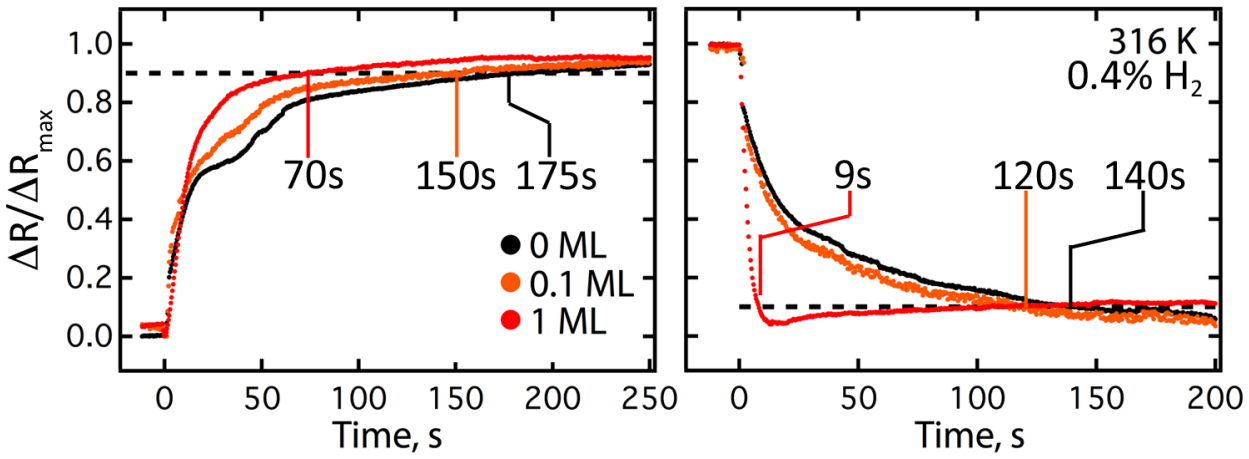

Figure 2.8: Normalized resistance change, $\Delta R/\Delta R_{max}$, *versus* time plots for the response (left) and recovery (right) of a Pd nanowire and two Pd@Pt nanowires showing response and recovery times. Shown are data for $\theta_{Pt} = 0$ ML (pure Pd), 0.1 ML, and 1.0 ML as indicated. $T = 316$K and the hydrogen concentration is 0.4% in air.

As shown in Fig. 7c, even one atomic layer of Pt causes a loss of sensitivity at 294K and 303K relative to 0.1 ML of Pt (Fig 7b), or no Pt (Fig 7a). For example, a Pd@Pt nanowire with $\theta_{Pt} = 1.0$ ML shows a LOD_{H_2} of 3000 ppm ($T = 294$K) whereas a pure Pd nanowire shows $\text{LOD}_{H_2} = 500$ ppm at the same temperature. At higher temperatures up to 376K, however, sensitivity disparities disappear: Both a Pd nanowire (Fig 7a) and a Pd@Pt nanowire with $\theta_{Pt} = 1.0$ ML (Fig 7c) show an equal loss in sensitivity to H_2 with increasing T. This heating-induced loss of sensitivity, seen previously for pure Pd nanowires operating in N_2,[77, 49] derives from the reduced solubility of H in Pd.[69, 37] For example, the equilibrium hydrogen partial pressure required to attain PdH_x for $0.1 < x < 0.6$ increases by a factor of ≈30 over the range from 294K to 376K.[69]

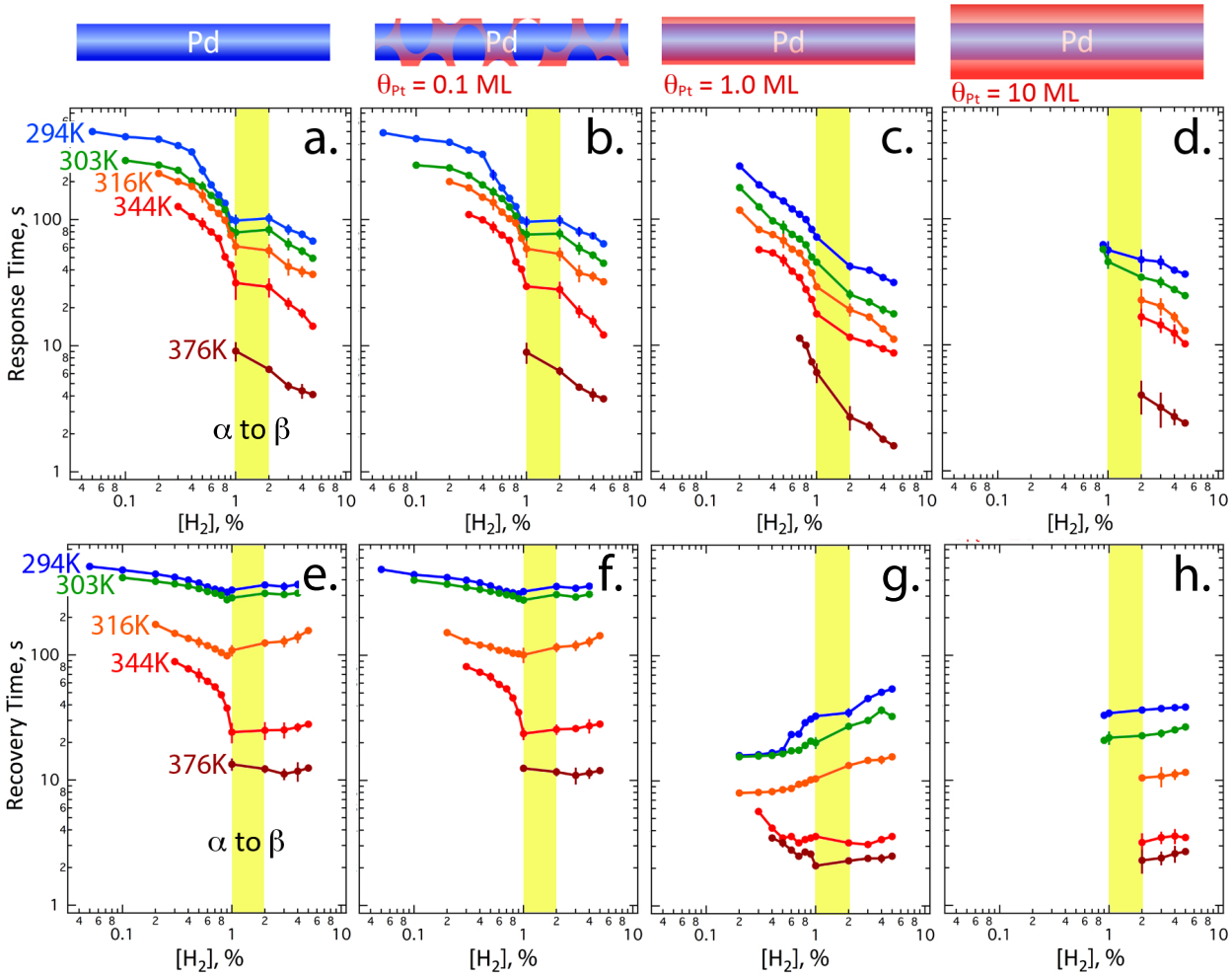

Figure 2.9: Response (a-d) and recovery (e-h) rate data for four nanowires, at five temperatures, as indicated: a,e) A Pd nanowire, b,f) A Pd@Pt nanowire with $\theta_{Pt} = 0.1$ ML., c,g) A Pd@Pt nanowire with $\theta_{Pt} = 1.0$ ML., and d,h) A Pd@Pt nanowire with $\theta_{Pt} = 10$ ML. The yellow region from 1-2% [H_2] coincides with the α-to-β phase transition of PdH_x.

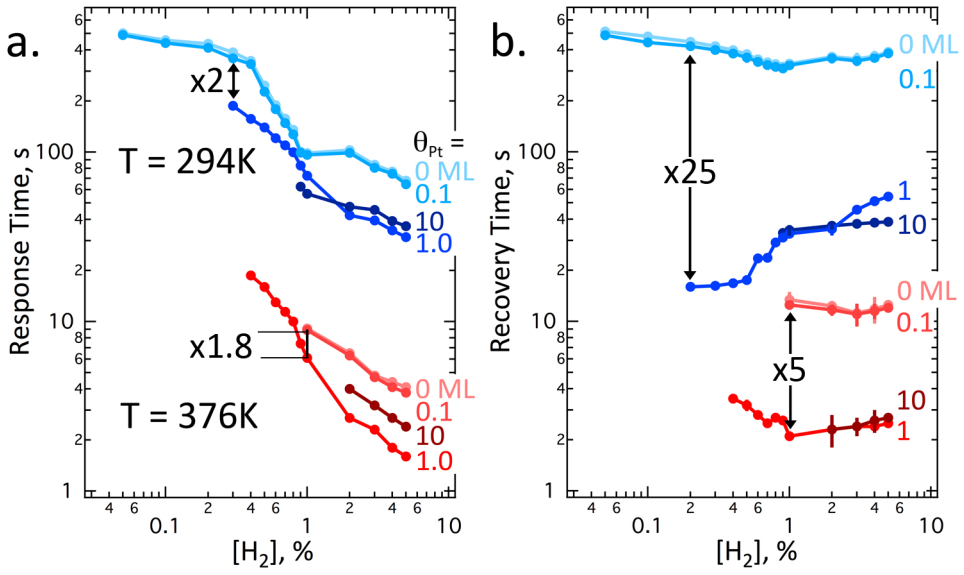

Figure 2.10: Influence of Pt coverage for Pd@Pt nanowires on the response and recovery of R at two temperatures, 294K and 376K: a) Response time *versus* [H_2]. The response times at both temperatures are decreased by a factor of ≈2 at the LOD_{H_2} as compared with a pure Pd nanowire operating at the same temperatures. b) Recovery time *versus* [H_2]. Sensor recovery times are decreased by a factor of 25 at 294K and by a factor of 5 at 376K at the LOD_{H_2}.

Increasing the Pt layer thickness to 10 MLs causes a more pronounced loss in sensitivity across all temperatures from 294K to 376K. A θ_{Pt} = 10 ML Pd@Pt nanowire shows a LOD_{H_2} = 1.0% at 294K (Figs 6c, 7d) and 2.0% at higher temperatures. Although, as described below, the response and recovery of a Pd@Pt nanowire with a 10 ML Pt surface layer is accelerated, the profound loss in sensitivity to H_2 is disabling with respect to the application of this nanowire as an H_2 sensor.

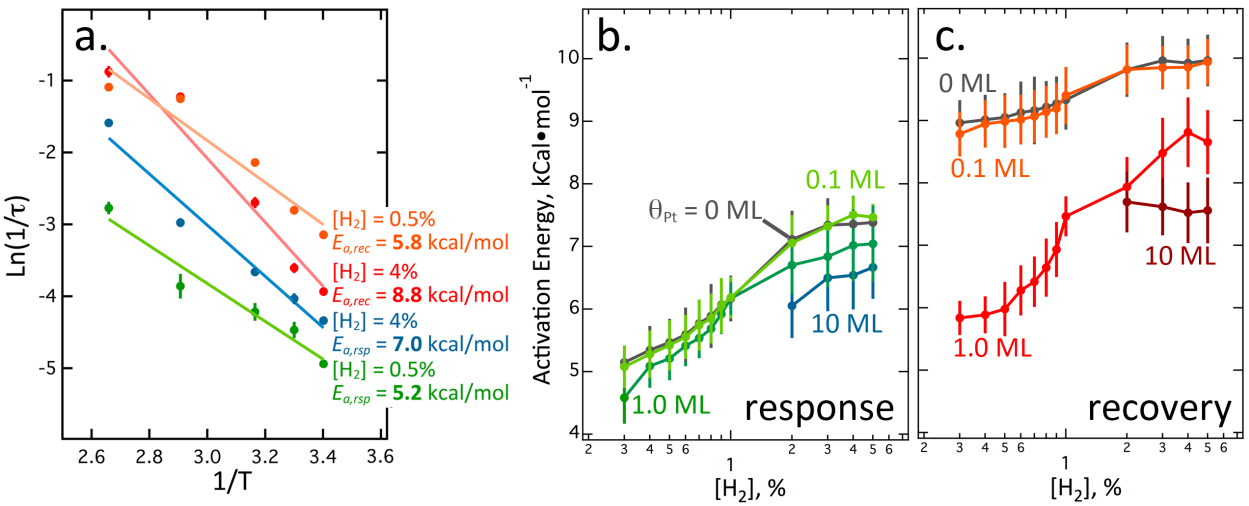

Figure 2.11: Arrhenius activation energy measurements for sensor response and recovery. a) Example of Arrhenius plots for the response and recovery of a Pd@Pt nanowire with θ_{Pt} = 1.0 ML at two H_2 concentrations: 4% and 0.5%, as indicated. b,c), $E_{a,resp}$ (b) and $E_{a,rec}$ (c) of Pd@Pt nanowire sensors as a function of H_2 concentration in air.

An examination of the raw R *versus* time data of Fig 6b shows that surface Pt can accelerate the response and recovery to H_2 in air for all temperatures in the range from 294K to 376K, relative to pure Pd (Fig 10). But θ_{Pt} = 0.1 ML is not enough - these Pd@Pt nanowires show a small, but insignificant acceleration of both response and recovery rates (Figs 10). Acceleration of the response and recovery *are* significant for both θ_{Pt} = 1.0 ML and 10 ML Pd@Pt nanowires.

For example, as shown in Fig. 10, the addition of 1.0 ML of Pt to the surface of a Pd nanowire accelerates the sensor response by a factor of ≈2 across all temperatures and H_2 concentrations (Fig 9c) relative to a pure Pd nanowire (Fig 9a). Recovery of the 1.0 ML of Pt sensor resistance after H_2 exposure is accelerated by an even larger factor of between 5, at 376K, and 20-25 at 294K (Fig 9g). The comparison of Fig 10 also shows that no significant difference between 1.0 ML and 10 ML of Pt is seen in either the response (Fig 9c,d) or recovery performance (Fig 9g,h), in spite of the fact that, as already noted, the sensitivity of the 10 ML Pd@Pt nanowire is depressed (Fig 7d).

Like a pure Pd nanowire, the response and recovery of a Pd@Pt nanowire are thermally activated and both processes are accelerated by Joule-heating (Figs 6,8)[77] Activation energies for sensor response, $E_{a,resp}$, and recovery, $E_{a,rec}$, can be derived from plots of $\ln(1/\tau)$ *versus* $1/T$ (*e.g.* Fig 11a) where τ is the response or recovery time, using the Arrhenius equation: $ln(1/\tau) = -E_a/RT + ln(A)$. At 376K, for example, sensor response is accelerated by one order of magnitude relative to 294K across all concentrations - a factor that is nearly identical to that measured for a pure Pd nanowire. $E_{a,resp}$ is unaffected by the platinum surface layer within our experimental error. This suggests that the rate-limiting chemical processes involved in sensor response are unaffected by the Pt surface layer. Since H_2 dissociation is rapid at both Pd and Pt surfaces, the barrier we measure may derive from the transition of a surface hydride species to a bulk hydride. We believe, however, that more rapid water formation by surface Pt is nevertheless responsible for depressing the sensitivity of Pd@Pt nanowires at low $T = 294$K and 303K. In contrast, the $E_{a,rec}$ is strongly influenced by surface Pt. For example, 1.0 ML of Pt causes a significant reduction in $E_{a,rec}$ across all concentrations. At 0.3%, for example, $E_{a,rec}$ is reduced from from 9 kcal/mol for pure Pd to 6 kcal/mol for a Pd@Pt nanowire with $\theta_{Pt} = 0.1$ ML. This reflects a change in the rate-limiting step for recovery at Pt-covered Pd@Pt nanowire which is explained by the increased activity of platinum for water formation.

2.3 Chapter Conclusions

The response/recovery speed of nanoscale chemical sensors is prone to retardation by rate-limiting surface chemical kinetics, because as the critical dimension of the sensor is reduced, the diffusional flux of molecules to sensor surfaces is increased. Diffusion limits are replaced by kinetic limits for surface chemical reactions that are involved in sensor function. For this

reason, the performance of nanoscale sensors should be hyper-sensitive to catalysts. This paper provides a graphic demonstration of this principle. We have demonstrated that H_2 response and recovery kinetics for a highly optimized H_2 sensor consisting of a Joule-heated Pd nanowire can be significantly accelerated by the addition of minute quantities (e.g. 1 ML) of a Pt metal catalyst to the nanowire surface, altering the kinetics of surface chemical reactions.

Specifically, a Pd@Pt nanowire alters the properties of Pd nanowire for detecting hydrogen, increasing the response speed by a factor of two at the limit-of-detection, and accelerating the recovery of the sensor in air by a factor of 2 - 25, depending on temperature. These changes apply to a coverage of Pt, θ_{Pt}, of 1.0 ML, the optimum coverage assessed here: A higher $\theta_{Pt} = 10$ MLs, causes a stronger loss of sensitivity to H_2, making it too insensitive for safety sensing purposes even though rapid response and recovery seen at the lower Pt coverage are retained. A lower $\theta_{Pt} = 0.1$ ML has no significant influence of sensitivity or the speed of response/recovery, even though this sub monolayer of Pt does alter the surface electrochemical response of the nanowire (Fig. 4). The benchmark that we use for this comparison is a Pd nanowire of the same size, which previously defined the state-of-the-art for resistor-based hydrogen gas detection.[72, 78, 77, 75]

As a footnote, we also demonstrate that a useful electrochemical method for depositing a conformal monolayer of Pt onto a Pd surface involving the use of very low electrodeposition rates. This process provides an alternative to the well-established surface-limited redox replacement (SLRR) process[16, 13, 47] for carrying out the conformal electrodeposition of a noble metal on the surface of another noble metal. Using this approach, we have electrodeposited ultra-thin layers (between 0.1 and 10 MLs) of Pt on Pd nanowire to create Pd@Pt core@shell nanowires with enhanced hydrogen gas detection capabilities.

2.4 Methods

2.4.1 Chemicals and Materials

Palladium chloride ($PdCl_2$, 99.999% trace metal basis), potassium hexachloroplatinate(IV) (K_2PtCl_6, 99.99% trace metal basis), ethylenediaminetetraacetic acid (EDTA, 99.995% trace metal basis), potassium chloride (KCl, 99.3%, ACS certified) were used as received from Sigma-Aldrich. Positive photoresist (Shipley S1808) and developer (Shipley MF-319) were purchased from Microchem Corporation. Acetone, methanol and nitric acid were used as received from Fisher (ACS certified). Nickel (Ni) and gold (Au) pellets (5 N purity) were used from Kurt J. Lesker Company for evaporation of films. Fast drying silver (Ag) paint was used as received from Ted Pella, Inc. Hydrogen gas (Airgas, purity $\geq$99.998%) and air (Airgas, purity $\geq$99.995%) were used as received.

2.4.2 Single Palladium (Pd) Nanowire Synthesis and Hydrogen Sensor Fabrication

Single palladium nanowire can be synthesized by lithographically patterned nanowire electrodeposition (LPNE) as described previously. Nickel films of 40nm thickness were thermally evaporated onto pre-cleaned 2 in. $\times$ 1 in. soda lime glasses, the thickness of nickel films was precisely measured by gold quartz crystal microbalance (QCM). The following step was to spin-coat a positive photoresist layer (Shipley S1808) at 2500 rmp for 80 seconds, and bake the photoresist in a constant temperature forced convection oven (Yamato Scientific America, Inc., model DKN 600) for 30 minutes at 90 ^{o}C. After the photoresist layer was cooled down to room temperature, it was mounted in contact with quartz photolithographic mask on photolithographic mask alignment fixture (Newport 83210). Then the photoresist layer was patterned by flood exposure UV light source (Newport model 97436, i-line, 365nm,

500 W x 3.00 s). The exposed photoresist was immersed in the developer (Shipley MF-319) for 20 seconds, rinsed with Millipore water (Milli-Q, p ¿ 18 MΩ · cm), and air dried. This sample was then exposed to 0.8 M nitric acid for 5 minutes to remove the nickel and also to produce a horizontal undercut beneath the protective photoresist layer. The height of this undercut was the same as the thickness of sacrificial nickel layer, and the width of the undercut produced by wet etching was ≈300 nm. The nickel edge of this horizontal trench was used as working electrode for the electrodeposition of a palladium nanowire.

A 100 mL one-compartment three-electrode electrochemical cell was used for single palladium nanowire electrodeposition. The aqueous plating solution contains 0.2 mM $PdCl_2$, 0.22 mM EDTA and 0.1 M KCl (Adjusted pH = 4.9). The whole photolithographically patterned template was immersed in plating solution while leaving the other edge of nickel out of the plating solution and connected to the potentiostat (Gamry Instrument, model G300). The counter electrode was a pre-cleaned 1 cm^2 platinum foil, and the reference electrode was saturated calomel electrode (SCE). Single palladium nanowire was electrodeposited at -0.80V vs SCE. When the electrodeposition was finished, the remaining photoresist layer was dissolved and rinsed off by acetone, and then nickel layer was etched away by 0.8 M nitric acid, leaving one single palladium nanowire adhering strongly to the glass surface. After the whole LPNE processes, as-made single palladium nanowire samples were thermally treated in nitrogen atmosphere at 200 °C for 2 hour by using a heavy duty tube furnace (Lindberg, model 54233).

2.4.3 Fabrication of Hydrogen Gas Sensor

Quasi four-probe contacts were made by thermally evaporating Au/ Cr (80nm/ 2nm) through shadow mask with 50 um gap on top of the nanowire. Silver paint was applied and sintered at 200 ^oC to connect Au/ Cr contacts to the gas flow cell. For platinum (Pt) electrodeposition,

another layer of photoresist (Shipley S1808) was spun on top of the as-made single nanowire sensor and baked as same as the previous LPNE processes. Then the sample was aligned with a photomask having a rectangle pattern of 25 μm wide and 1 in. long, and then shifted horizontally for multiple photolithographic exposures, which were finished by the same flood exposure UV light source. After photoresist development, single Pd nanowire was exposed as working electrode for Pt electrodeposition. Then, Au/Cr contacts were covered by photoresist and Pt electrodeposition on the exposed Pd nanowire was carried out using a three-electrode electrochemical cell. The aqueous plating solution consisted of aqueous 0.1 mM K_2PtCl_6 and 0.1 M KCl.

2.4.4 Scanning Electron Microscopy (SEM)

Scanning electron micrographs were acquired by using a FEI Magellan 400 XHR system. Energy dispersive spectroscopic (EDS) images were acquired by same SEM system with EDS detector (Oxford Instruments, 80 mm^2, with Aztec software). Accelerating voltages of electron beam ranged from 1 kV to 5 kV, and probe currents ranged from 1.6 pA to 0.4 nA. All the SEM specimens were mounted on stainless stubs and held by copper clips.

2.4.5 X-ray Photoelectron Spectroscopy (XPS)

The surface chemical compositions of Pd@Pt nanowires was determined using X-ray photoelectron spectroscopy (XPS) using a ESCALAB MKII surface analysis instrument (VG Scientific) equipped with a twin anode x-ray source (Mg/Al) and a 150 mm hemispherical electron energy analyzer. XPS spectra were collected under the base pressure of the spectroscopy chamber around 3×10^{-10} Torr using Al Kα with X-ray (1486.6 eV) in constant energy mode, a pass energy of 20 eV, an energy step of 50 meV and an acquisition time for both Pd 3d and Pt 4f of 3s. Binding energies were calibrated using the C 1s peak of adventi-

tious carbon at 284.6 eV as a reference and the Au $4f_{7/2}$ at 84.0 eV from gold foil physically attached to the sample surface. Using XPSPEAK software with Shirley-type background functions, Pd 3d XPS spectra were fit with spin-orbit doublets ($3d_{5/2}$ and $3d_{3/2}$) at a fixed intensity ratio (3:2). We assign the features of Pd $3d_{5/2}$ spectra at BE 335.7 eV as metallic Pd and 337.6 eV as to Pd^{4+} species, such as PdO_2. Pt 4f XPS spectra were fit with spin-orbit doublets ($4f_{7/2}$ and $4f_{5/2}$) at a fixed intensity ratio (4:3). We assign the features of Pt $4f_{7/2}$ spectra at BE 71.2 eV as metallic Pt and 72.8 eV as to Pt^{2+} species, such as PtO or $Pt(OH)_2$. Furthermore, using an atomic sensitivity factor of 5.356 for Pd 3d, 5.575 for Pt 4f, and 0.339 for Si 2p, we further estimate the relative peak concentrations of Pd 3d and Pt 4f normalized to the Si 2p from glass substrate.

2.4.6 Thermal Calibration

An infrared furnace (ULVAC- RIKO, Inc., Model MILA-5000 Infrared Lamp Rapid Annealing System) was programmed to ramp temperature in the range of 293 K to 393 K. The *in-situ* resistance measurement of a 50 μm-length single Pd nanowire (40 nm $\times$ 200 nm) was determined using a sourcemeter (Keithley Instrument, model 2400) and a multimeter (Keithley Instrument, model 2000) in a nitrogen atmosphere. Sample data are available in the Supporting Information.

2.4.7 Theoretical Simulation

COMSOL Multiphysics (Version 4.3a) was used for finite element modeling of the Joule-heating temperature profile along a 50 μm- length nanowire (40 nm $\times$ 100 nm). The applied module was joule-heating.

2.4.8 Hydrogen Sensing

Single nanowire sensors were mounted in a sealed flow cell (dead volume = 120 μL), equipped with two gas input channels, one for a H_2:air mixture and the other for pure air. The H_2:air mixture was prepared by mixing H_2 with air at known ratios, established by mixing these two gases at controlled gas flow rates produced by mass flow controllers (MKS Inc., model 1479A). Two fast valves (Parker Valve, cycle time = 25 ms) metered pulses of H_2:air into the flow cell, and synchronously interrupted the flow of air during the pulse. All hydrogen sensing experiments were accomplished using dry gases at ambient laboratory temperature (about 20°C) and a total gas flow rate of 1500 sccm. These two valves and three mass flow controllers were all controlled using LabView in conjunction with a National Instruments interface (model BNC 2110) and a computer. The nanowire resistance was measured in a four-terminal configuration using a combination of a source-meter (Keithley Instruments, model 2611A) and a multi-meter (Keithley Instruments, model 2000). The source meter supplied a voltage that fixed the nanowire temperature according to the calibration curve for that particular nanowire (*vide supra).*

2.5 Acknowledgement

The authors gratefully acknowledges the financial support of this work by the National Science Foundation Division of Chemistry CHE-0956524. Work by Yu Liu and John C. Hemminger was supported by the U.S. Department of Energy, Office of Science, Basic Energy Sciences under Award DE-FG02-96ER45576. SEM data were acquired using instrumentation of the *LEXI* facility (lexi.eng.uci.edu/) at UCI.

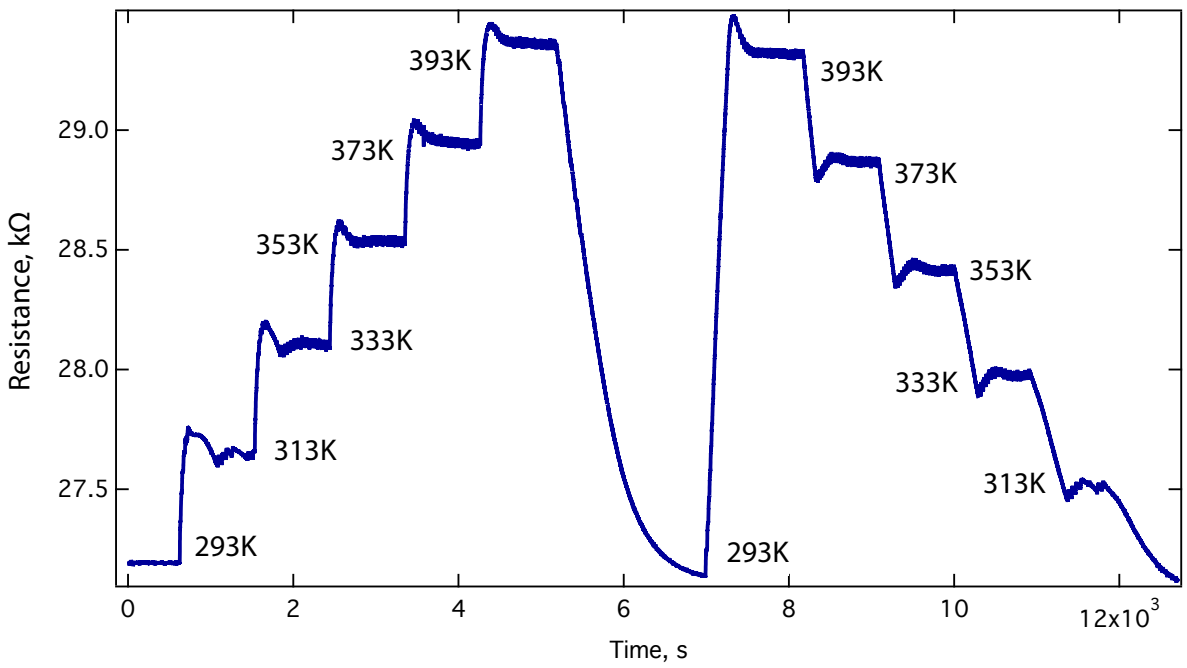

Figure 2.12: In-situ resistance measurement of a thermally heated single Pd@Pt nanowire. The dimension of the nanowire is 40 nm (h) × 100 nm (w) × 50 μm (l). The temperature of the rapid annealing system is programmed to range from 293 K to 393 K, at a step rate of 20 K and stabilized at each temperature step for 10 min.

2.6 Supporting Information: Temperature Measurement of Single Pd@Pt Nanowire

2.6.1 Thermal Calibration

As stated in the experimental section, an infrared furnace (ULVAC- RIKO, Inc., Model MILA-5000 Infrared Lamp Rapid Annealing System) is connected to lab computer and programmed in CX-Thermal to ramp temperature in the range of 293 K to 393 K. The in-situ resistance measurement of a single Pd@Pt nanowire (40 nm (h) × 100 nm (w) × 50 μm (l)) was finished by using a source-meter (Keithley Instrument, model 2400) and a multimeter (Keithley Instrument, model 2000) in the atmosphere of nitrogen.

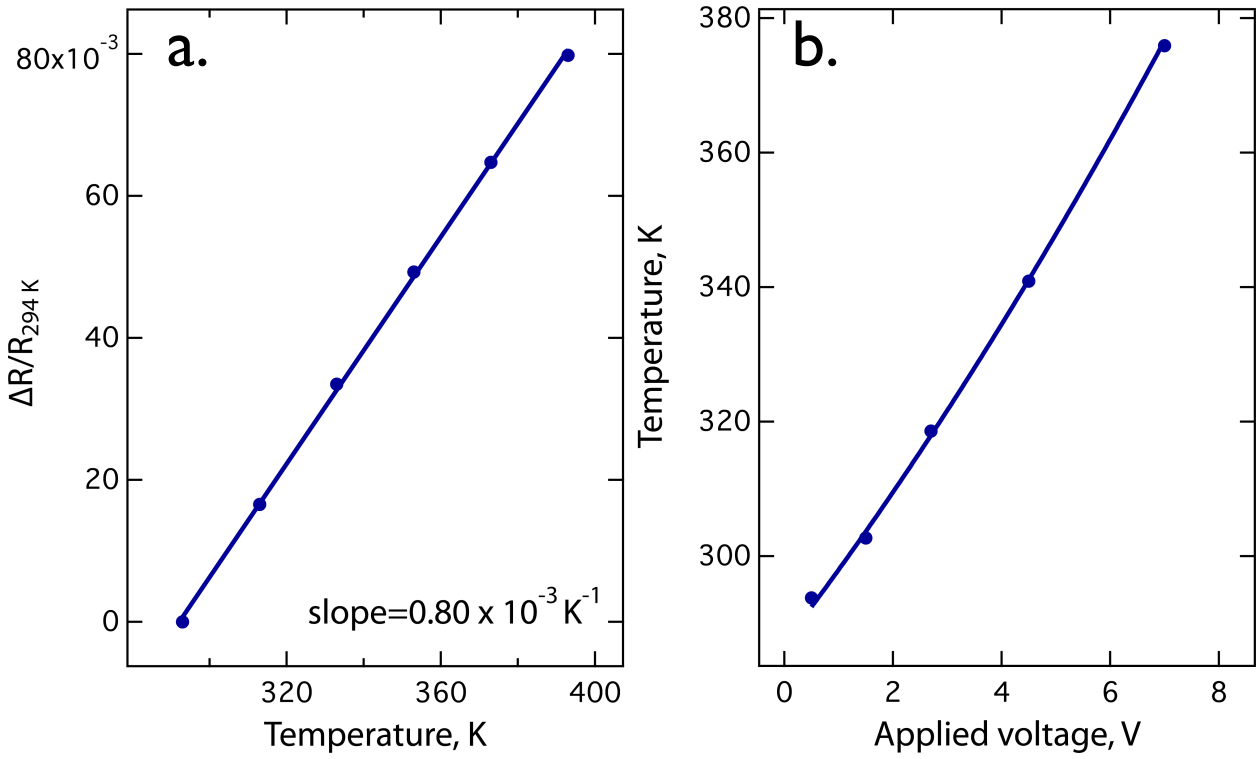

Figure 2.13: Correspondence of applied voltages to working temperature along single Pd@Pt nanowire. a) The rates of resistance increase caused by thermal heat are calculated and plotted versus applied temperature, and the temperature coefficient of resistance α is indicated. b) The applied Joule-heating voltages correspond to different working temperature along the single Pd@Pt nanowire by the temperature coefficient of resistance calculated from (a).

2.6.2 Calculation of Joule-Heating Temperature

The ratio of resistance increase caused by thermal heat is plotted versus applied temperature of the infrared furnace, and then temperature coefficient of resistance α is calculated. Joule-heating voltages have been applied to single Pd@Pt nanowires, resulting in the baseline increase of resistance, which means the resistance of nanowire without being exposed to hydrogen. The temperature increase caused by Joule-heating is calculated by using α, and related to the applied voltage along the nanowires.

Table 2.1: Department of Energy (DOE) Target Metrics Governing Performance for Hydrogen Gas Sensors[a].

Parameter	DOE Target
Sensitivity	25% (1 vol% H_2)
Range and Accuracy	0.1 - 4%, ±1% of full scale over the lifetime of the sensor
Lifetime	5 years
Response Time	<1 min at 25% LFL[b] (1 vol%)
	<1 sec at 100% LFL (4 vol%)
Recovery Time	60 sec.

[a]Source: DOE Energy Efficiency & Renewable Energy 2009 Hydrogen Sensor Workshop.
[b]LFL = Lower Flammability Limit.

Table 2.2: Performance Metrics for Fast, Resistance-Based Hydrogen Sensors Operating in Nitrogen.

Sensing Element[a]	Critical Dimensions	Temp ^{o}K	$\tau_{resp} : \tau_{rec}$ $[H_2] \approx 0.1\%$ [b]	$\tau_{resp} : \tau_{rec}$ $[H_2] \approx 4\%$ [c]	LOD_{H_2} [d]	Ref
in Nitrogen						
Fractured Pd nanowire	d = 200-250nm	RT	n.r.	0.07s : 0.07s	1-2%	[7]
Pd film nanogap	t = 10-100nm	RT	n.r.	52s : 122s	2%	[29]
Pd nanowire	d = 50-80 nm	RT	15s : n.r.	12s : n.r.	27 ppm	[49]
Pd film nanogap	t = 6-10nm	RT	n.r.	0.5s : 0.5s	1-2%	[34]
Pd film nanogap	t = ∼10nm	RT	n.r.	5-10s : 200s	0.5%	[30]
Pd nanoparticle film	t = 3.3nm	RT	10s : 10s	0.07s : 0.07s	25 ppm	[73]
Pd nanowire	33 (h)×47nm(w)	RT	40s : 300s	30s : 100s	2 ppm	[78, 75]
Pd nanowire	27 (h)×75nm(w)	428	7s : 15s	2s : 6s	200 ppm	[77]
Pd nano-network	d = 1-3 nm	RT	30s : n.r.	3-4s : n.r.	1000 ppm	[80, 81]

[a]Abbreviations: RT = room temperature, t = thickness, d = diameter, (h) × (w) are the lateral dimensions of a nanowire with a rectangular cross section., n.r. = not reported.
[b]$R_{initial}$ to $0.90R_{max}$ response time.
[c]R_{max} to $0.10R_{max}$ recovery time.
[e]a Pt nanowire does not discriminate concentration across its entire response range.

Table 2.3: Performance Metrics for Fast, Resistance-Based Hydrogen Sensors Operating in Air.

Sensing Element[a]	Critical Dimensions	Temp ^{o}K	τ_{resp} : τ_{rec} $[H_2] \approx 0.1\%$ [b]	τ_{resp} : τ_{rec} $[H_2] \approx 4\%$ [c]	LOD_{H_2} [d]	Ref
in Air						
Pd/Ni film	t = 50nm	RT	120s : 20s	20s : 100s	n.r.	[22]
Pd nanowire	d = 50-80nm	RT	n.r.	n.r.	1000 ppm	[49]
Pd nanowire	25 (h)×85nm(w)	RT	400s : 1000s	100s : 200s	100 ppm	[78, 75]
Pt nanowire[e]	20 (h)×130nm(w)	550	150s : 1100s	1s : 1100s	10 ppm	[74]
Pd@Pt nanowires						
θ_{Pt} = **0 ML**	40 (h)×100nm(w)	294	450s : 480s	80s : 380s	500 ppm	**this work**
	”	376	n.r.	4.5s : 10s	1%	”
θ_{Pt} = **0.1 ML**	”	294	150s : 1100s	80s : 380s	500 ppm	”
	”	376	n.r.	4s : 10s	1%	”
θ_{Pt} = **1.0 ML**	”	294	250s : 15s	35s : 50s	0.2%	”
	”	376	n.r.	2s : 2.5s	0.4%	”
θ_{Pt} = **10 ML**	”	294	n.r.	40s : 40s	0.9%	”
	”	376	n.r.	3s : 2.5s	2%	”

[a]Abbreviations: RT = room temperature, t = thickness, d = diameter, (h) × (w) are the lateral dimensions of a nanowire with a rectangular cross section., n.r. = not reported.
[b]$R_{initial}$ to $0.90R_{max}$ response time.
[c]R_{max} to $0.10R_{max}$ recovery time.
[e]a Pt nanowire does not discriminate concentration across its entire response range.

Chapter 3

Palladium Nanoparticle-Decorated Carbon Nanotube Ropes for Rapid, Sensitive H_2 Detection

3.1 Introduction

Sensors capable of detecting hydrogen gas in air are important for the detection of leaked hydrogen,[3, 54] for control of chemical processes in industry,[21, 31] and for investigations of physiological processes.[6, 70] Chemiresistors are amongst the simplest chemical sensor architectures. Hughes and Schubert[22] demonstrated the first chemiresistor for H_2 gas in 1992, consisting of an evaporated palladium-nickel alloy film resistor. These simple devices produced a rapid response to H_2 exposure of several seconds (at 4%) but were not able to detect hydrogen in air at low concentrations, below 0.1%. Nanowire chemiresistors[39, 77, 75, 78, 80, 49] accelerated response and recovery to H_2, relative to the results of Hughes and Schubert, but the limit-of-detection for H_2 in air ($LOD_{H_2} \approx 0.05\%$ at RT)[39] was

only slighted improved compared with Pd-Ni film chemiresistors ($LOD_{H_2} \approx 0.1\%$).[22] The following discussion pertains specifically to hydrogen gas detection in an air background.

Since the observation in 2000[9] that the electrical conductivity of single walled carbon nanotubes (SWCNTs) is strongly affected by ambient gas composition, carbon nanotubes (CNTs) have been extensively studied as components of chemiresistive sensors. CNTs decorated with Pd and Pt[42, 33, 27] nanoparticles, were evaluated as H_2 sensors by multiple research groups (Table 1). Insights into the mechanism of H_2 sensing in these systems are provided by experiments conducted by Collins and coworkers[28] in which a pristine, defect-free, semiconducting SWCNT was compared with SWCNTs containing a single defect. In that work, H_2 exposure induced a resistance increase of ≈50% for pristine SWCNTs decorated by many palladium nanoparticles. But SWCNTs with a single defect, decorated with a single palladium nanoparticle, were far more sensitive transducers of H_2 exposure, producing a resistance increase of three orders of magnitude. These experiments demonstrated for the first time that SWCNTs with defects are capable of amplifying the chemiresistive response to H_2.[28] The response to H_2 of graphene-supported with Pd and Pt nanoparticles has also been studied and metrics for response/recovery speed and LOD_{H_2} are similar to those obtained for SWCNTs (Table 1) and, as in the case of SWCNTs, are also highly variable.[68, 27, 8] A third category of sensors exploit palladium Schottky contacts, but no dispersed Pd or Pt particles, to enable H_2 detection at either CNTs or graphene.[82, 7]

An important problem seen in many previous studies involving both graphene[68] and CNT-based sensors[10, 35, 8] is that exposure to H_2 does not yield a steady-state, time invariant change in electrical resistance. Instead, an increasing resistance is observed during H_2 exposures, sometimes lasting minutes, independent of the H_2 concentration. For many graphene and CNT-based devices, the sensor resistance either does not stabilize at all,[10, 8] or it fails to do so on a useful time scale.[8] Pd nanowires, in contrast, do not exhibit this problem.[39, 77, 75, 78, 80, 49]

To summarize, with a few exceptions, palladium nanowires are capable of functioning as chemiresistors for H_2 that respond and recover rapidly in air but are relatively insensitive.[39, 77, 75, 78, 80, 49] Pd-decorated SWCNTs and graphene can be highly sensitive, but are usually slow - even failing in many cases to produce a time-invariant resistance change (Table 1). However the liabilities seen for graphene-based and SWCNT-based H_2 sensors may simply be a consequence of the method of palladium deposition onto these supports. While several methods have been used to deposit palladium on these nanocarbon supports - including physical vapor deposition, chemical (electroless) deposition,[27, 33, 41] electrodeposition,[35] and the deposition of Pd or Pt colloids[42] - the properties of the metal nanoparticles has not been subjected to optimization - in terms of the particle size monodispersity, the mean nanoparticle diameter, and the chemical state of the nanoparticle surface (whether stabilized or not). The hypothesis explored in this paper is that these metrics determine both the H_2 sensing speed and LOD_{H_2}. To test this hypothesis, we have prepared single semiconducting-CNT ropes using dielectrophoresis and decorated these with Pd using a pulsed electrodeposition procedure that produces sub-10 nm diameter Pd nanoparticles that are both unstabilized and narrowly dispersed in diameter (RSD = 8-12%). The resulting chemiresistors enable the detection of H_2 with response/recovery times in air at room temperature that are faster than single palladium (Pd) nanowires or Pd nanoparticles dispersed onto nanocarbons, while enabling a much great dynamic range spanning 3.5 decades in H_2 concentration (Table 1).

3.2 Results and Discussion

3.2.1 Pd-CNTs hydrogen sensors fabrication and characterization

Hydrogen sensors were prepared using a variant of the lithographically patterned nanowire electrodeposition (LPNE) method (Figure 1).[72, 71, 43] LPNE was first used to prepare

a single, linear CNT rope by pulsed, dc-dielectrophoresis (Figure 1, steps 1-5). This CNT rope was 100 μm in total length, and several microns in width. In prior work, patterned CNT ropes and rope arrays have been obtained by dielectrophoresis[32, 61] using a variety of templates.[59, 60, 44] Alignment of individual CNTs with the axis of the rope is generally obtained because this direction coincides with the direction of the electric field gradient in the system,[59, 60, 44] but more disordered ropes have been obtained when the electric field gradient driving deposition is oriented orthogonal to the axis of the deposited rope.[61] This circumstance also exists for the deposition of CNT ropes using LPNE (Figure 2) and such ropes were used in this study. As seen in Figure 2d, a 50 μm length was electrically isolated using evaporated gold contacts on a 2 nm thickness adhesive chromium interlayer (Figure 1, steps 6-9).

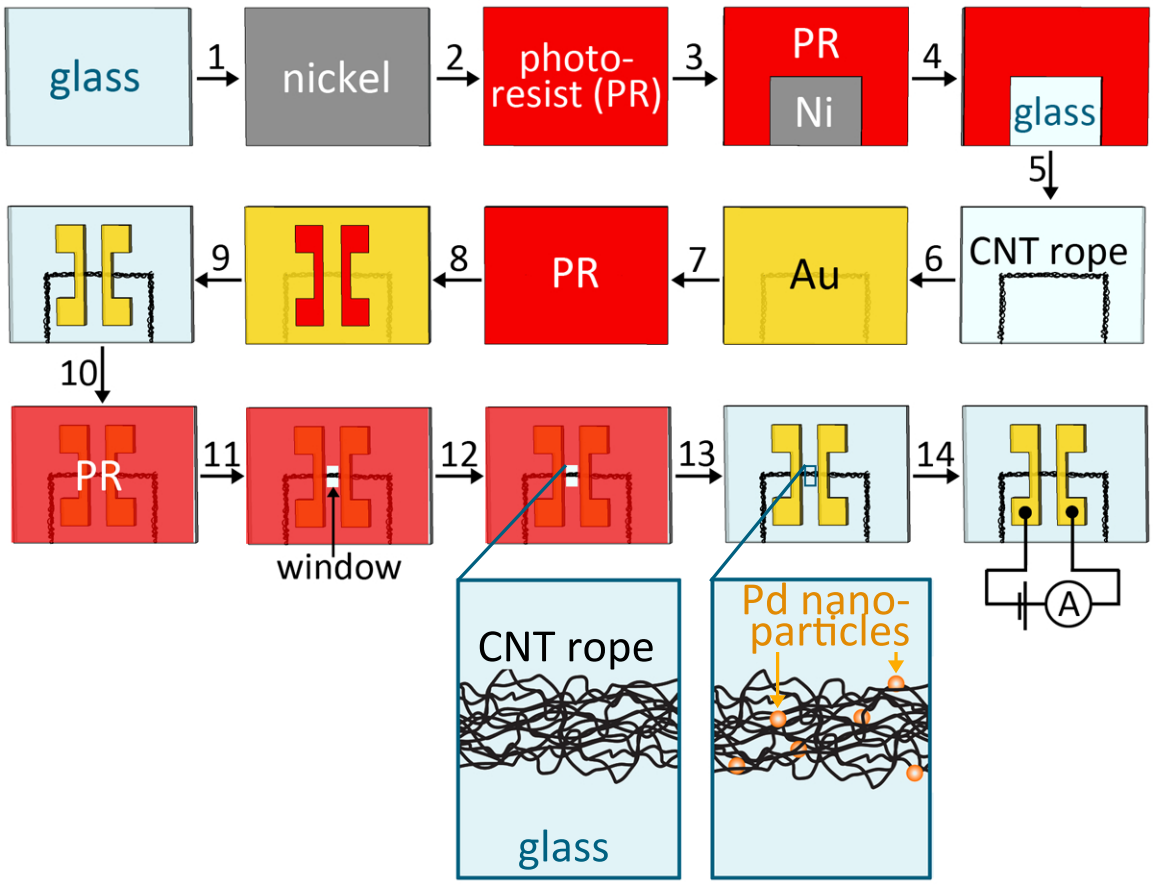

Figure 3.1: Process flow for the fabrication of a palladium nanoparticle decorated carbon nanotube rope (Pd-CNT rope) H_2 sensor. Each process step is described in the Materials and Methods section.

Pd nanoparticles were then electrodeposited onto the 50 μm length section of CNT rope located between these two gold contacts (Figure 1, steps 10-13) using a multi-pulse electrodeposition scheme (Figure 3). Cyclic voltammograms for a single CNT rope in an aqueous palladium plating solution show an onset for a irreversible reduction at 0.0V vs. SCE and an overpotential for palladium deposition, η_{Pd}, on scan 1 of $\approx$ -300 mV. η_{Pd} is the additional voltage, beyond the Nernst potential for Pd^{2+} reduction, that is required to form Pd^{o} nuclei on CNT surfaces. Both Pd^{2+} reduction and hydrogen evolution can be expected to occur concurrently at this potential, and both are irreversible processes (Figure 3a). Pd nanoparticles were prepared on CNT ropes in this solution by applying voltage pulses of -0.80 V (vs. SCE) $\times$ 100 ms separated by 2s wait times at 0.0 V (Figure 3b). This pulsed deposition scheme is designed to maximize the number density of Pd nanoparticles produced within the CNT rope because each pulse exceeds η_{Pd} while the wait time between pulses allows Pd^{2+} ions to diffusively back-fill after each pulse. Since Pd nanoparticle nucleation is first order in $[Pd^{2+}]$, refreshing the Pd^{2+} should enable the highest possible nucleation rate, resulting in size similar nanoparticles with a diameter that is correlated with the total coulombic loading. A plot of current and integrated charge *versus* time (Figure 3c) show the preponderance of cathodic current and the build-up of cathodic charge at every voltage pulse. With successive pulses, the current amplitude increases somewhat (Figure 3d), consistent with the electrocatalysis of both H_2 evolution and Pd^{2+} reduction by the Pd nanoparticles. This autocatalysis is also observed in the cyclic voltammograms shown in Figure 3a which show increasing peak currents on three successive voltammetric scans. Because the Pd^{2+} reduction current is augmented by H_2 evolution, the coulombic loading we measure, Q_{Pd}, provides an upper limit on the actual Pd loading onto the CNT rope. Q_{Pd} values of 15 μC to 102 μC were investigated here. The electrodeposited Pd nanoparticles distributing on the CNT sidewalls were charatecterized by using high-resolution transmission electron microscope (HRTEM) (Figure 4a), there were $\approx$ 40 nanoparticles found within the area of 120 nm $\times$ 120 nm, the element of was identified by EDX (Figure 4b). The mean diameters

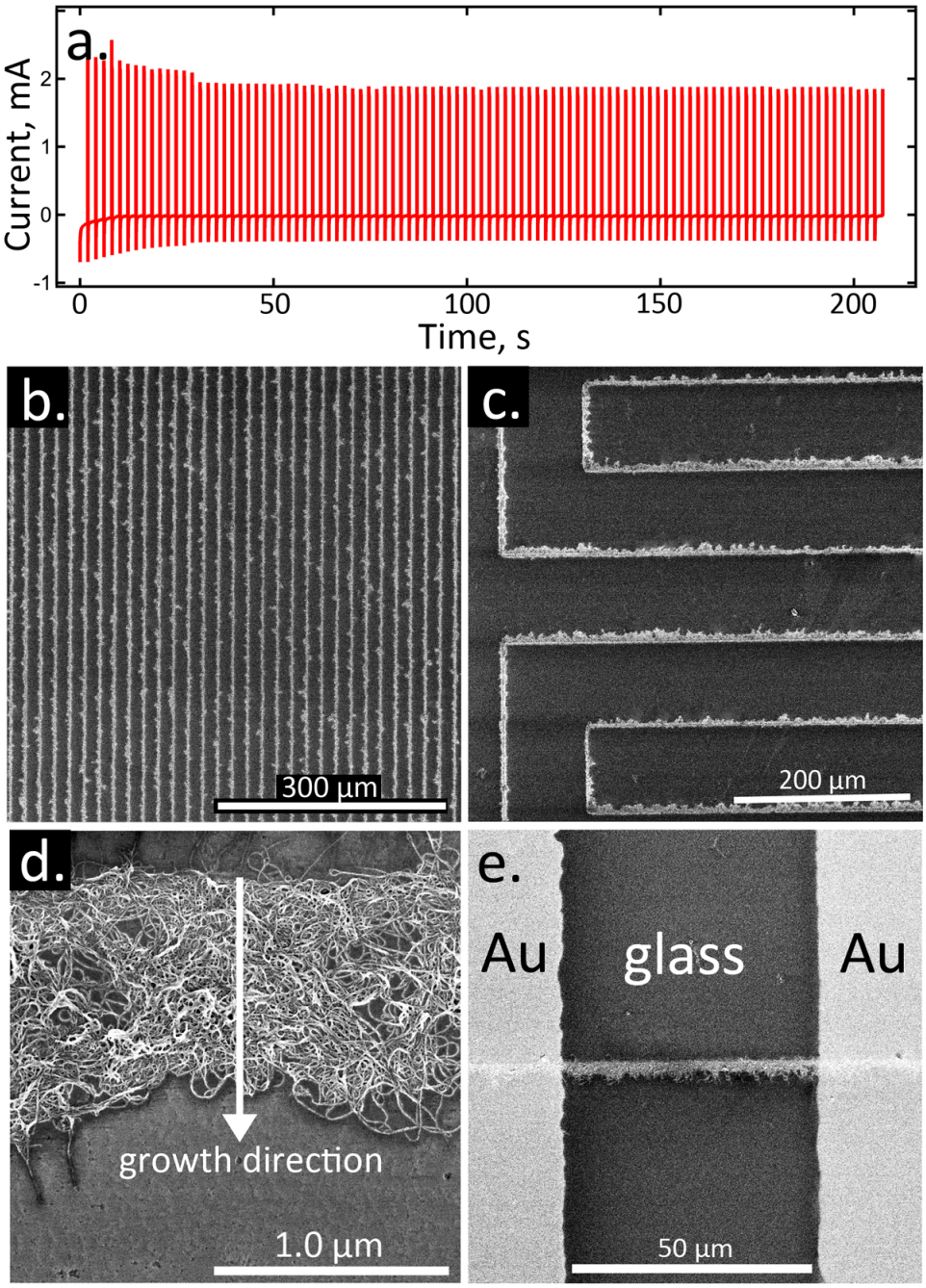

Figure 3.2: Patterning of CNT ropes prepared by LPNE-templated dielectrophoresis. a) Current *versus* time for the dielectrophoretic deposition of CNT ropes at an LPNE-patterned template induced by a train of +20 V × 0.10s pulses separated in time by 1.0 s. b) Scanning electron micrograph (SEM) of an array of CNT ropes on glass patterned at 20 μm pitch using LPNE. c) SEM image of loops of CNT rope patterned at 100 μm pitch using LPNE. d) Higher magnification SEM image of a section of CNT rope 1.0 - 1.5 μm in width. e) A Pd-CNT rope H_2 sensor consisting of a single CNT rope decorated with Pd nanoparticles (not visible in this image) and evaporated gold electrical contacts.

of Pd nanoparticles ranged from 4.5 (± 1) nm to 5.8 (± 3) nm (Figure 4c). Compared with prior research on electrodepositing Pd nanoparticles on CNTs, this method of pulsing depositing potential took advantages of forming large amount of small yet seperated nanoparticles rather than continuous microfilms. Both density of nanoparticles in unit area and mean diameter increased for larger Q_{Pd}, however, the mean diameter changed slightly even for higher coulombic depostion charge, due to that the Pd nanoparticles dimension was highly dependent on the applied potential for electrodeposition[11].

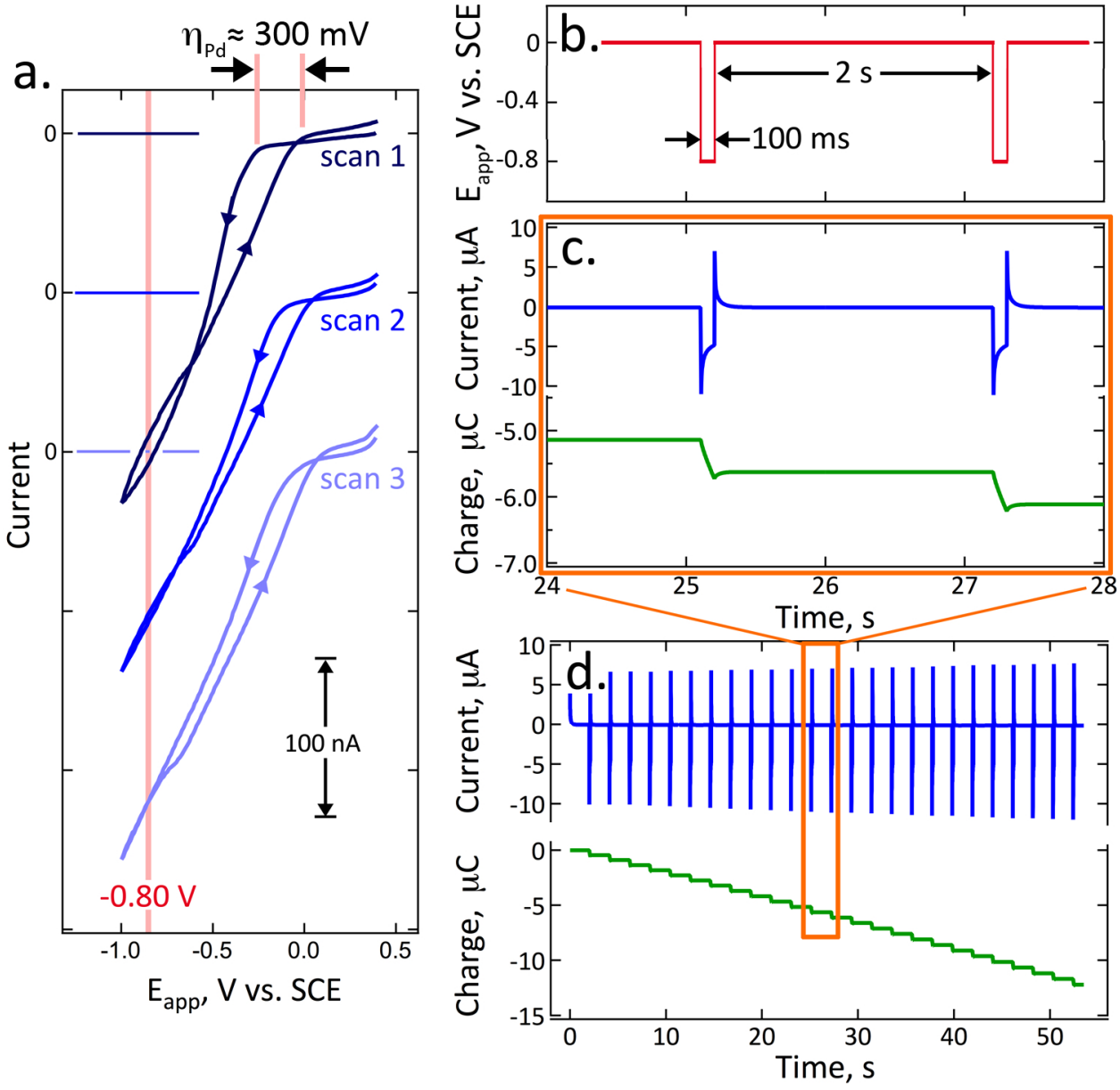

Figure 3.3: Electrodeposition of Pd nanoparticles onto CNT ropes. a) Cyclic voltammograms at 20 mV/s in aqueous 0.2 mM $PdCl_2$, 0.22 mM EDTA, 0.1 M KCl showing reduction of Pd^{2+} and concurrent H_2 evolution. b) Pd nanoparticles were electrodeposited onto a single CNT rope by applying a train of potential pulses of -0.80 V vs. SCE, using the pulse program shown here. c) Current (blue trace) and charge (green trace) versus time for two deposition pulses illustrating the build-up of cathodic charge corresponding to both Pd reduction (Pd^{2+} + $2e^- \rightarrow Pd^0$) and H_3O^+ reduction ($H_3O^+ + 2e^- \rightarrow H_2 + OH^-$).

3.2.2 Hydrogen gas detection in air

Four sets of Pd-CNT rope chemiresistive sensors were tested by applying bias of 0.5 V - 1 V for the application of detecting H_2 balanced in air, all of the sensors responded to H_2 exposure in a dynamic range from 10 ppm to 40,000 ppm (4%) at room temperature (Figure 5). Semiconducting CNTs of chirality (6, 5) exhibited no obvious reponse to H_2 mixture from 100 ppm to 1000 ppm, and sensitivity to H_2 was induced dramatically with electrodeposited Pd nanoparticles. For the Pd-CNT sensors with $Q_{Pd} = 15$ μC, they showed saturation states upon exposure to H_2 even at low concentrations of H_2. The sensors with higher coulombic loading behaved with much larger signal change of $\Delta R/ R_0$ but reached no steady states particularly for low concentrations. Another drawback for putting more Pd loading was to slow down the rate of response and recovery. Although the mean diameter changed from 4.5 nm to 5.8 nm in terms of increasing the coulombic loading from 15 μC to 102 μC, the Pd particles with the diameter of $\approx$ 8 - 10nm existing in the highest coulombic loading can act as the bottleneck for dragging down the speed of detecting H_2. If the Pd-CNT rope H_2 sensors were compared to a single Pd nanowire sensor published previously with the dimension of 40 nm (h) $\times$ 100 nm (w) $\times$ 50 μm (l)[39], the least sensitive Pd-CNT sensors exhibited $\Delta R/ R_0$ at $[H_2] = 1000$ ppm that was $\approx$ 30 times higher than observed for the case of a single Pd nanowire working at room temperature (Figure 6). According to previous published results, single Pd nanowire H_2 sensors can be accelerated at higher working temperatures induced by self Joule-heating, yet the sensitivity and detection deteriorate dramatically. We compared H_2 sensing performance of single Pd nanowire sensors at three different working temperatures to all Pd-CNT sensors, the coulombic loading of Pd on CNT ropes is a critical factor affecting H_2 detection, both response and recovery decelerate for higher coulombic loading of Pd nanoparticles. The lowest loading $Q_{Pd} = 15$ μC exhibits faster response and recovery rates than Pd nanowire sensors working at 294 K and 316 K for all H_2 concentrations. Single Pd nanowire sensors surpass H_2 sensing performance of Pd-CNT sensors at 376 K, however,

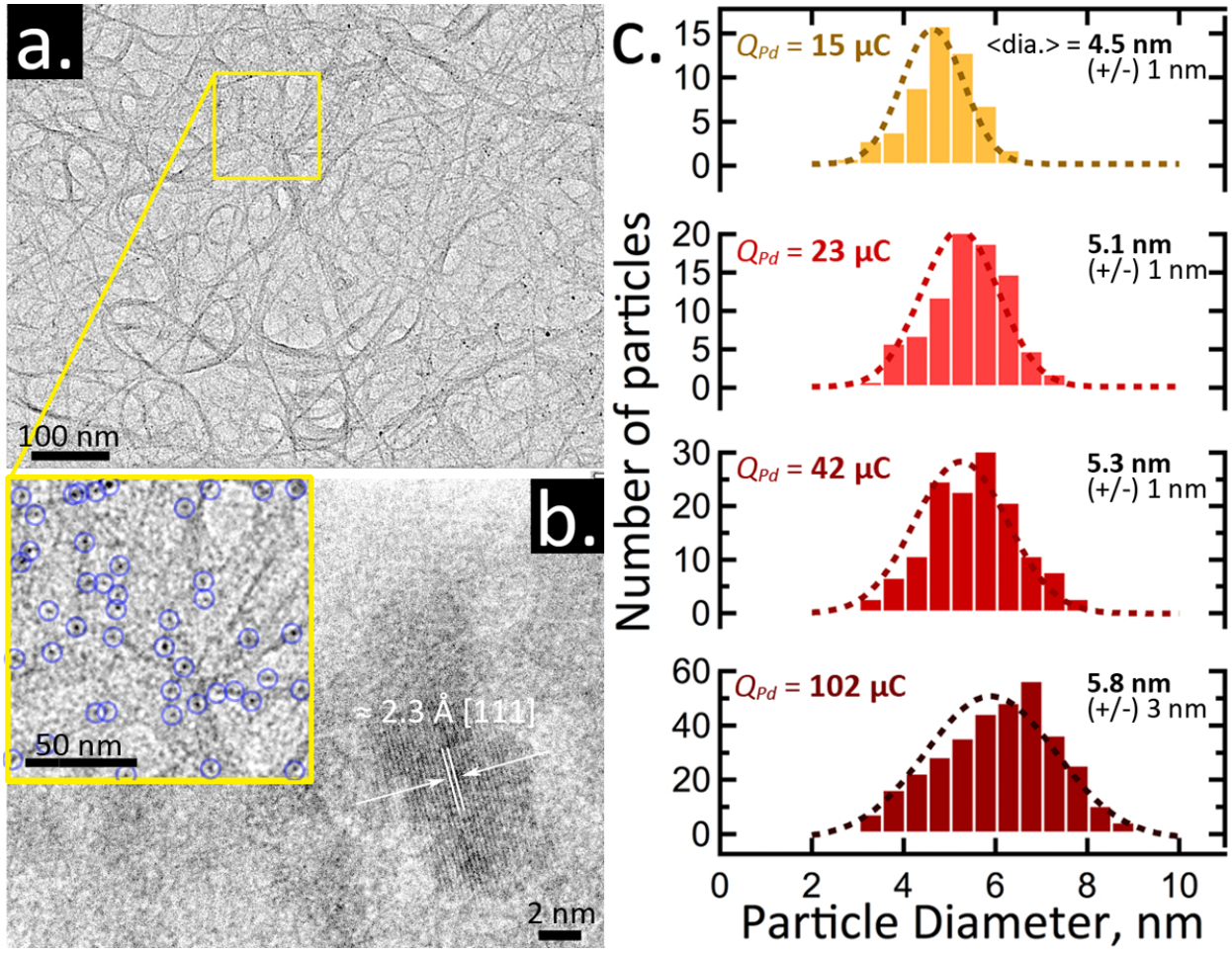

Figure 3.4: TEM characterization of electrodeposited Pd nanoparticles. a) Low magnification TEM image of a CNT rope after the deposition of palladium nanoparticles (Q_{Pd} = 42 μC). Palladium nanoparticles are distributed across this entire image, with some of the largest seen as dark spots in the lower right corner of this image. b) (Inset) Higher magnification view of the region shown in yellow in (a),. Blue circles highlight ≈40 Pd nanoparticles present in this region. A high resolution TEM image of one of these nanoparticles is shown in the main image. c) Histograms of Pd nanoparticle diameters obtained from TEM analysis of either 2 or 3 sensors prepared using the indicated Q_{Pd} (Table 2).

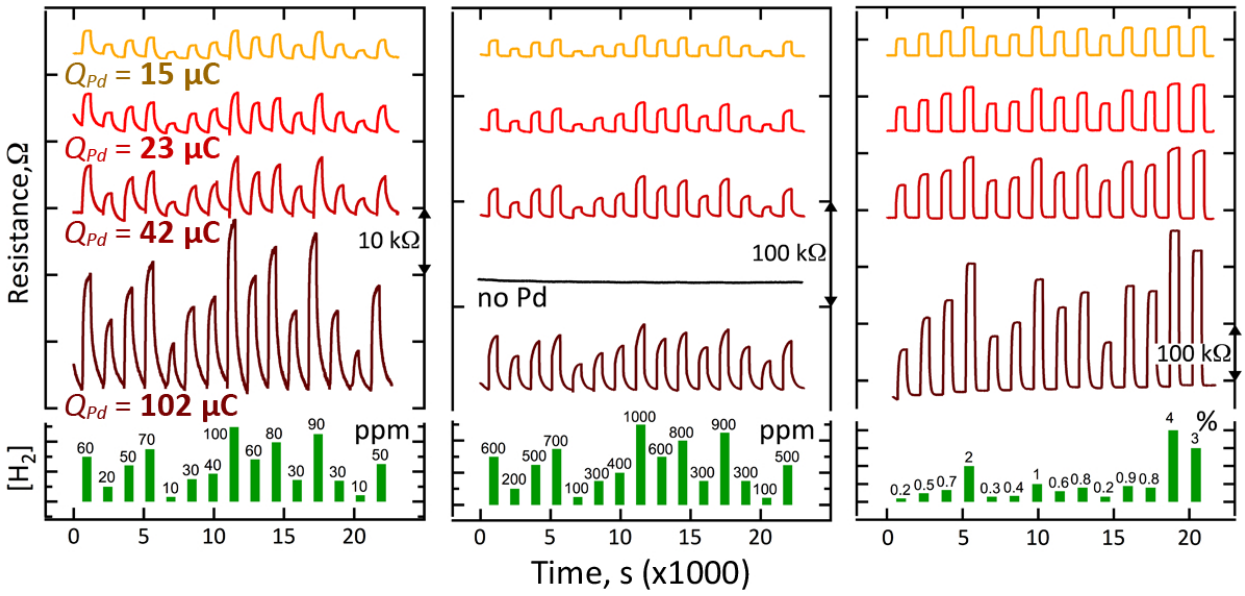

Figure 3.5: Pd-CNT rope sensor responses, for sensors prepared using four coulombic loadings of Pd, as indicated. Three $[H_2]$ concentration ranges are shown: **Left**, 10 ppm < $[H_2]$ < 100 ppm; **Middle**, 100 ppm < $[H_2]$ < 1000 ppm, **Right**, 0.2% < $[H_2]$ < 4%.

working at such high temperature leads to the disadvantage of losing sensitivity and detection limit from 500 ppm to 10,000 ppm.

The process of fabricating Pd-CNT sensors produces many defects on the sidewall of CNTs, but there is no direct evidence to quantitatively estimate the amount of defect on CNT ropes, although they are randomly distributed with the CNT ropes. Pd nanoparticles show the preferences to be electrodeposited on such defect sites rather than pristine parts on side walls[11], and the chemiresistive signal, in other words, amplification of resistance change upon H_2 exposure can be strongly enhanced in comparison with either Pd nanoparticles on pristine CNTs[28] or solid Pd nanowires[39]. The metal-semiconductor barrier existing at the interjunction between Pd nanoparticles and CNTs acts as a variable resistor, the barrier height is highly dependent on the work function of Pd nanoparticles, which can be lowered by adsorbed gas molecules[64], resulting in partially neutralizing the majority carriers within semiconducting CNT ropes. In order to quantitatively explain the mechanism, we need to make an assumption that the variation of work function of Pd nanoparticles would be correlated to the surface fraction (γ) occupied by disassociated H_2 at different concentrations, thus chemiresistive signal change is proportional to γ ($\Delta R \propto \rho$, $\Delta R/ R_0 \propto \gamma$) and Langmuir adsorption isothem theory can be applied for explaining the enhanced H_2 sensing at Pd nanoparticles on CNT ropes. H_2 gas molecules can be disassociated as:

$$H_2 + 2Pd_{surface} \rightarrow 2Pd_{surface}H$$

Here $Pd_{surface}$ denotes the active sites on surface of Pd nanoparticles. If we define the surface area of a single Pd nanoparticle as S_0, the adsorption and desorption constant as k_{ad} and k_{de} respectively, and partial pressure of H_2 balanced in air as ρ, then the adsorption and desorption rate are:

$$rate_{ad} = k_{ad}\ \rho\ (1 - \gamma)^2\ {S_0}^2$$

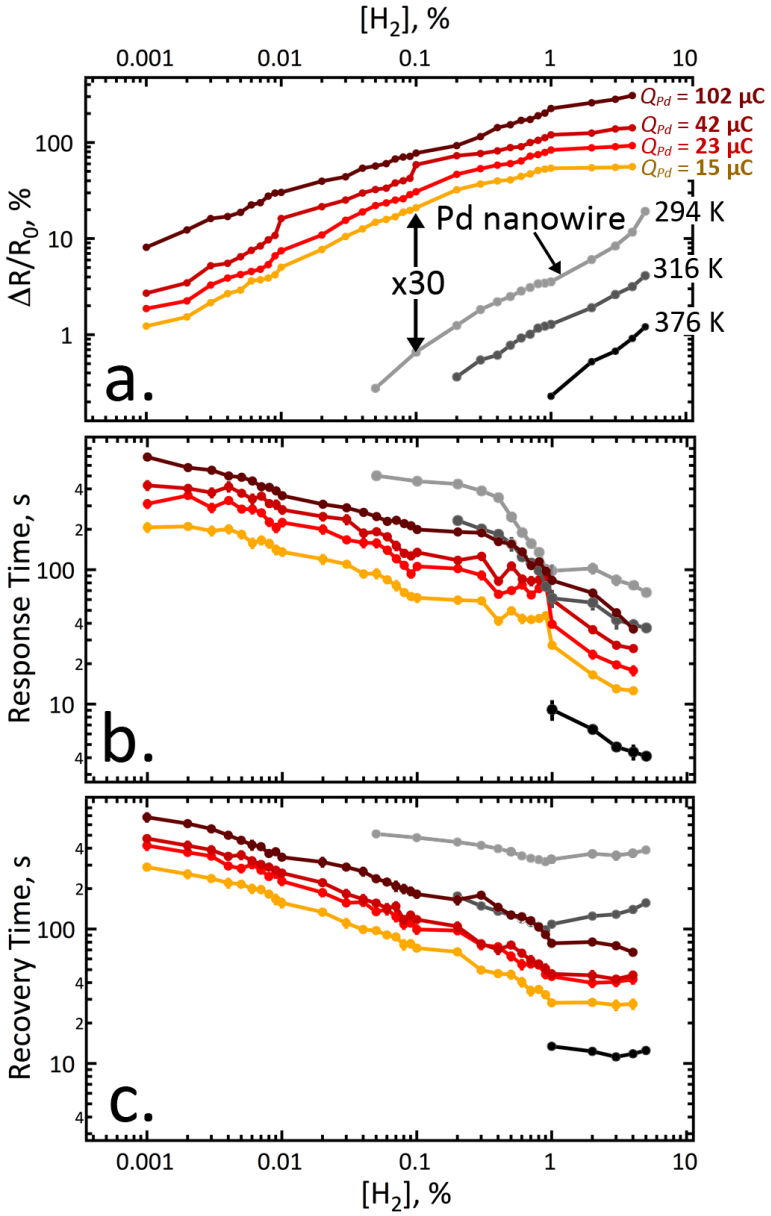

Figure 3.6: Hydrogen sensing metrics for Pd-CNT rope H_2 sensors, and a comparison to a single Pd nanowire sensor (40 nm × 100 nm × 50 μm) operated at three temperatures.[39] a) $\Delta R/R_0$, the relative resistance change, *versus* [H_2] in air for five sensors, as indicated. Parameters for the Pd-CNT rope H_2 sensors as summarized in Table 2. $\Delta R/R_0$ increases monotonically with Pd loading, and the mean Pd particle diameter. The least sensitive Pd-CNT rope ($Q_{Pd} = 15$ μC) exhibits a $\Delta R/R_0$ response at [H_2] = 1000 ppm that is thirty times higher than observed for a Pd nanowire at 294 K. A LOD_{H2} ¡ 10 ppm is obtained for all four Pd-CNT rope H_2 sensors. b) Response time *versus* [H_2] in air, and, c) Recovery time *versus* [H_2] in air for the same five sensors described in (a).

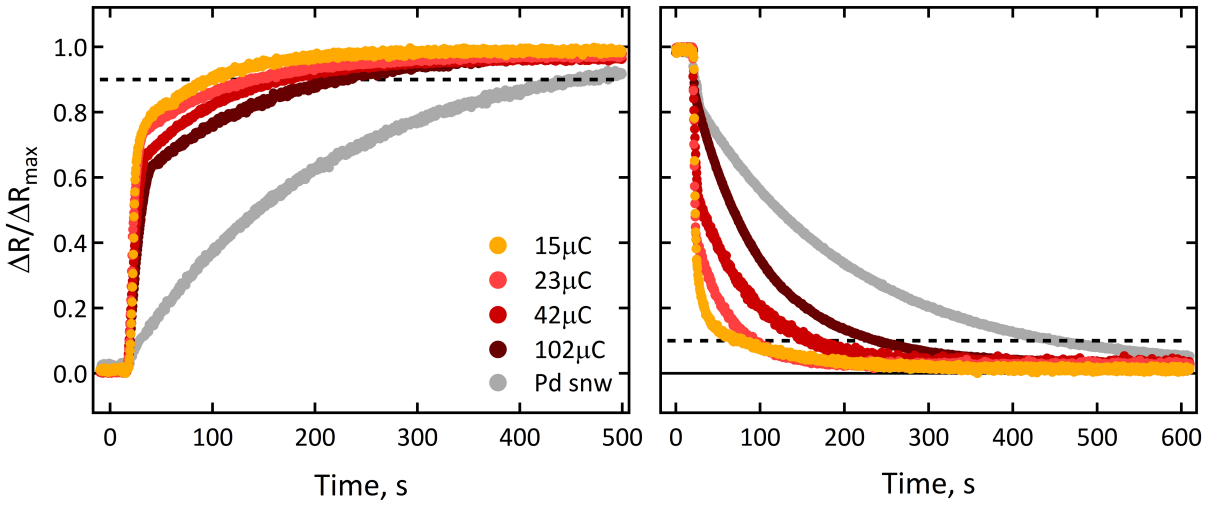

Figure 3.7: Comparison of a single Pd nanowire H_2 sensor (40 nm (h) × 100 (w) × 50 μm (l)) and Pd-CNT sensors with four coulombic loading of Q_{Pd} = 15 μC, 23 μC, 42 μC, 102 μC upon 1000 ppm H_2 exposure.

$\text{rate}_{de} = k_{de}\ \gamma^2\ {S_0}^2$

In case that the Pd-CNT sensors reach equilibrium, in other words, chemiresistance change is at the steady saturation state upon expure to a certain H_2 concentration, adsorption rate approximately equals desorption rate by:

$k_{ad}\ \rho\ (1 - \gamma)^2\ {S_0}^2 = k_{de}\ \gamma^2\ {S_0}^2$

$\gamma/\ (1 - \gamma) = (k_{ad}/\ k_{de})^{1/2}\ \rho^{1/2}$

For low H_2 concentration mixture ($\leq$ 10,000 ppm), hydrogen coverage at Pd nanoparticles surface is also very low (ρ ¡¡ 1), then the approximation can be made as:

$\gamma/\ (1\text{-}\gamma) \approx \gamma$

$\Delta R/\ R_0 \propto \gamma \approx (k_{ad}/\ k_{de})^{1/2}\ \rho^{1/2}$

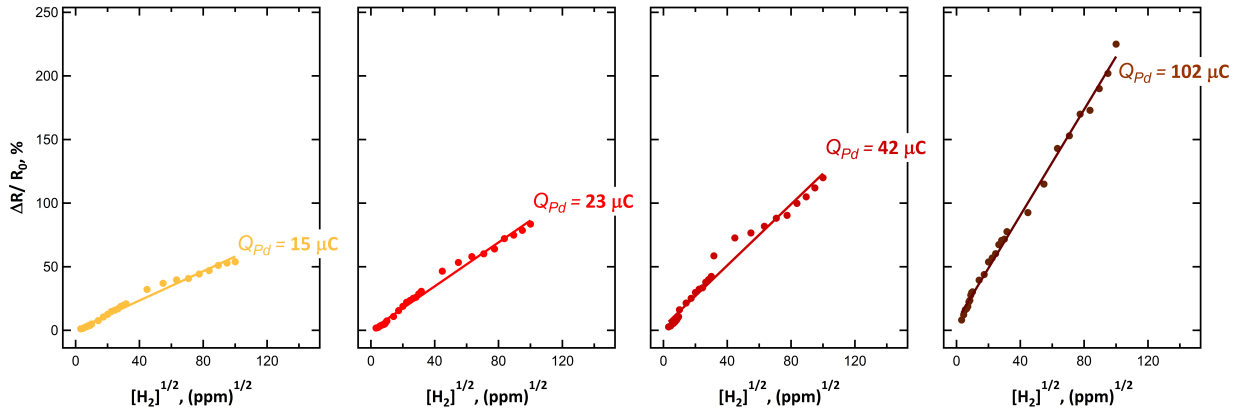

Figure 3.8: Chemiresistive signal changes of Pd-CNT sensors (as $\Delta R/ R_0$) with four coulombic loadings upon exposure to square root of H_2 concentration ranged from 10 ppm to 10,000 ppm (1%). From left to right, electrodeposited Pd nanoparticles of Q_{Pd} = 15 μC, 23 μC, 42 μC, 102 μC.

So the chemiresistance change upon H_2 exposures should be proportional to the squar root of H_2 partial pressure or concentration. The experimental data generated from CNT ropes with different Pd loadings falls in the regions of linear correlation (Figure 8).

3.3 Chapter Conclusions

Inches long semiconducting CNT ropes are deposited along the lithographically patterned nanoelectrodes by the processes of dielectrophoresis. The critical dimension and geometry of CNT ropes can be well controlled in terms of varying the applied DC voltage and duration of dielectrophoresis processes. CNT ropes decorated with electrodeposited Pd nanoparticles of four different coulombic loadings (Q_{Pd} = 15 μC, 23 μC, 42 μC, 102 μC) are evaluated for detecting H_2/ air mixture concentrated in the dynamic range from 10 ppm to 40,000 ppm (4%) at room temperature, all the Pd-CNT sensors exhibit fast and distinguishable responses corresponded to altered H_2 concentrations. The mean diameter increment of Pd nanoparticles is ¡ 2 nm with respect to maintaining the overpotential for electrodeposition yet increasing the coulombic deposition charge from 15 μC to 102 μC, however the variation of Pd nanoparticles diameter enlarged, leading to decelerated H_2 detection.

We have demonstrated that the chemiresistance induced by H_2 exposures in air can be amplified by electrodeposited Pd nanoparticles on CNT ropes, particularly in comparison with single Pd nanowires as benchmarks. For the CNT ropes loaded with Q_{Pd} = 15 μC Pd nanoparticles, the signal amplification is 3 – 30. For all H_2 concentrations, response and recovery time are faster than single Pd nanowire sensors working at 294 K and 316K. The Pd-CNTs sensors are extremely sensitive to H_2 by detecting H_2 in air as low as 10 ppm, regarding that the lowest detection limit of single Pd sensors is 500 ppm.

3.4 Methods

3.4.1 Chemicals and Materials

Single-wall carbon nanotubes ((6, 5) chirality, carbon ≤95%, ≥93% as SWNTs, diameters ranged in 0.7-0.9 nm measured by fluorescence), palladium chloride ($PdCl_2$, 99.999% trace metal basis), ethylenediaminetetraacetic acid (EDTA, 99.995% trace metal basis), potassium chloride (KCl, 99.3%, ACS certified), and sodium dodecyl sulfate (SDS, ≥99.0%, ACS reagent) were used as received from Sigma-Aldrich. Positive photoresist (Shipley S1808) and developer (Shipley MF-319) were purchased from Microchem Corporation. Acetone, methanol and nitric acid were used as received from Fisher (ACS certified). Nickel (Ni) and gold (Au) pellets (5 N purity) were used from Kurt J. Lesker Company for films evaporation.

3.4.2 Electrophoretic Deposition of Single SWNTs Bundles

The aqueous solution for SWNTs electrophoretic deposition contains 10 mg/L SWNTs and 0.1 g/L SDS, the solution was sonicated for 6 hours prior to the experiments to disperse carbon nanotubes. The procedures of electrophoretically depositing SWNTs shared parts of the experimental procedures of lithographically patterned nanowire electrodeposition (LPNE) as described in previous publications. Nickel films of 40nm thickness were thermally evaporated onto pre-cleaned 3 in. × 1 in. soda lime glasses, the thickness of nickel films was precisely measured by gold quartz crystal microbalance (QCM). The following step was to spin-coat a positive photoresist layer (Shipley S1808) at 2500 rmp for 80 seconds, and bake the photoresist in a forced convection oven (Yamato Scientific America, Inc., model DKN 600) at constant 90 ^{o}C for 30 minutes. After the photoresist layer was cooled down to room temperature, it was mounted in contact with quartz mask on photolithographic mask alignment fixture (Newport 83210). Then the photoresist layer was patterned by a flood exposure UV

light source (Newport model 97436, i-line, 365nm, 500 W $\times$ 3.00 s). The whole region of exposed photoresist was immersed in the photoresist developer (Shipley MF-319) for 20 seconds and rinsed off by Millipore water (Milli-Q, $\rho > 18$ M$\Omega \cdot$ cm), then dried by compressed lab air. The whole sample was dipped in 0.8 M nitric acid for 5 – 10 minutes, in order to etch away exposed nickel region and produce a horizontal undercut beneath the protective photoresist layer, and the height of this undercut was exactly same as the thickness of sacrificial nickel layer. The nickel edge of this undercut was used as working electrode for electrophoretically depositing SWNTs bundles.

A 50 mL one-compartment two-electrode electrochemical cell was used for electrophoretic SWNTs deposition. The photolithographically patterned Ni electrode was immersed in aqueous solution of dispersed SWNTs while leaving the other edge of nickel out of the solution and connected to a sourcemeter (Keithley Instruments, model 2611A) or potentiostat (Gamry Series G300). The counter electrode was a pre-cleaned 1 cm^2 platinum foil. SWNTs bundles were electrophoretically deposited by applying series of pulsed potentials. For each applied pulse in case of a sourcemeter was employed, the applied potential was 20 V, pulse duration was 0.1 s and relaxation time between two continuous pulses was 2 s, the total pulse number is 100. For the case when a Gamry potentiostat was employed, the applied potential was 10 V, pulse duration was 0.05 – 0.1 s and the total pulse number is 100. The width of SWNTs bundles can be well controlled by changing such abovementioned parameters. When the deposition was finished, the remaining photoresist layer was completely dissolved and rinsed off by acetone, and then nickel layer was totally etched away by 0.8 M nitric acid, leaving one single SWNTs bundle adhering strongly to the glass surface.

3.4.3 Electrochemical Decoration of Pd Nanoparticels and Fabrication of Hydrogen Gas Sensor

A second step of thermal metal evaporation and photolithography were applied for making electrical contacts. The procedures are: First, a layer of 2 nm Cr was thermally evaporated onto the as-made single SWNTs bundles, followed by the second thermal metal evaporation of 80 nm Au. Then a layer of S1808 photoresist was spun coated and baked for photolithography as described previously. After the photoresist layer was patterned, the uncovered part of Au/ Cr layers was etched away, leaving patterned metallic layers on both sides of a 50μm-long single bundle SWNTs. For Pd nanoparticles electrodeposition on SWNTs, it was carried out in a three-electrode electrochemical cell with saturated calomel electrode (SCE) as reference electrode, the aqueous plating solution contains 0.2 mM $PdCl_2$, 0.22 mM EDTA and 0.1 M KCl. The Pd nanoparticles were electrodeposited by pulsing applied potential as well. For each pulse, the applied potential was -0.8 V vs. SCE, the pulse duration was 0.1 s. The pulse cycle numbers were varied from 50 to 400, then the transient faradaic current was integrated and calculated as the total charges.

3.4.4 Scanning Electron Microscopy (SEM)

Scanning electron micrographs were acquired by using a FEI Magellan 400 XHR system. Energy dispersive spectroscopic (EDS) images were acquired by the same SEM system with EDS detector (Oxford Instruments, 80 mm^2, with Aztec software). Acceleration voltages of incident electron beams ranged from 1 kV to 5 kV, and probe currents ranged from 1.6 pA to 0.4 nA. All the SEM specimens were mounted on stainless stubs and held by copper clips.

3.4.5 Transmission Electron Microscopy (TEM)

Transmission electron micrographs were acquired by using high resolution mode of a Philip CM-20 system operating at 200 kV acceleration voltage. Carbon nanotubes bundles with Pd nanoparticles were held by copper TEM grids coated by 3 nm amorphous carbon films.

3.4.6 Hydrogen Sensing

As-fabricated Pd@SWNTs sensors were mounted in a sealed flow cell (120 μL), which had two gas-flow channels, one for hydrogen (Airgas, purity $\geq$ 99.998%) / dry air (Airgas, purity $\geq$ 99.995%) mixture and the other for purging air. The resistance of sensors was measured in situ when the sensors were exposed in mixed hydrogen gas flow. The resistance measurement setup contained a source-meter (Keithley Instruments, model 2611A) and a multi-meter (Keithley Instruments, model 2000). Flow controllers (MKS Inc., model 1479A) were used to control gas flow rates and pre-mixed hydrogen in air for a predetermined concentration. The switching valves (Parker Valve, switch time = 25 ms) of both mixing and purging channels were connected to a National Instruments interface (model BNC 2110) in conjunction with a computer. The gas flow processes were programmed and controlled by Labview programs. All hydrogen sensing experiments were finished by using dry gases at ambient laboratory temperature (about 20 ^{o}C) and total gas flow rate was maintained constantly at 1000 sccm.

3.5 Acknowledgement

The authors gratefully acknowledge the financial support of this work by the National Science Foundation, Division of Materials Research through contract DMR-1206867. FE-SEM and TEM data were acquired using the instrumentation of the LEXI (lexi.eng.uci.edu/) and IMRI (ps.uci.edu/imri/) facilities at UCI.

Table 3.1: Performance Metrics for Resistance-Based Hydrogen Sensors Operating in Air.

Sensing Element[a]	Sensor Type	Sensing Range	$\tau_{resp} : \tau_{rec}$ [b] (s)	@[H_2] (ppm)	LOD_{H_2} [c] (ppm)	Ref
Pd@SWNTs	ChemFET	200 – 1000 ppm	300 : 500	1000	200	[7]
Pd@SWNTs	ChemFET	25 – 2000 ppm	160 : 500	1000	25	[82]
Pt@RGO	ChemFET	1 – 100 ppm	50 : 100	50	1	[36]
Pd@RGO	Chemiresistor	20 – 1000 ppm	300 : 1500	1000	20	[8]
Pt/SnO_2@RGO	Chemiresistor	5000 ppm – 3%	70 : 40	10000	5000	[56]
Pd@Carbon nw	Chemiresistor	10 – 500 ppm	200 : 800	500	10	[40]
Pd/Ni@SWNTs	Chemiresistor	200 ppm – 1.6%	300 : 500	2000	200	[41]
Pd/Pt@MWNTs	Chemiresistor	400 ppm – 4%	150 : 200	1000	400	[53]
Pd@DWNTs	Chemiresistor	500 ppm – 3%	180 : 220	1000	500	[55]
Pd@SWNTs	Chemiresistor	30 ppm – 1%	280 : 300	1000	30	[63]
Pd@SWNTs	Chemiresistor	100 ppm – 2%	950 : 3300	1000	100	[45]
Pt s-nw	Chemiresistor	10 ppm – 4%	180 : 1300	1000	10	[74]
Pd s-nw	Chemiresistor	500 ppm – 4%	435 : 445	1000	500	[39]
Pt@Pd s-nw	Chemiresistor	500 ppm – 4%	264 : 120	2000	500	[39]
Pd@SWNTs	**Chemiresistor**	**10 ppm – 4%**	**62 : 72**	**1000**	**10**	**this work**

[a] Abbreviations: SWNT = single walled carbon nanotubes, RGO = reduced graphene oxide, nw = nanowire, DWNT = double walled carbon nanotubes, s-nw = single nanowire.
[b] τ_{resp}, τ_{rec} are response time ($R_{initial}$ to $0.90R_{max}$) and recovery time (R_{max} to $0.10R_{max}$) respectively.
[c] LOD_{H_2}: Limit of detection for hydrogen.

Table 3.2: Parameters for Palladium Nanoparticle-Decorated CNT Rope (Pd-CNT Rope) Hydrogen Sensors.

Q_{Pd}[a] (μC)	Number of Sensors	Pd particle dia. (nm)	R_0[b] (kΩ)	$\tau_{resp} : \tau_{rec}$[c] (s : s)	$(\Delta R/R_0)_{1000ppm}$[d] (%)
15 ($\pm$ 1)	3	4.5 ($\pm$ 0.8)	91	62 : 72	21 ($\pm$ 2)
23 ($\pm$ 1)	3	5.1 ($\pm$ 0.9)	89	106 : 100	31 ($\pm$ 1)
42 ($\pm$ 1)	2	5.3 ($\pm$ 1.3)	86	135 : 118	59 ($\pm$ 5)
102 ($\pm$ 3)	2	5.8 ($\pm$ 2.8)	80	200 : 182	78 ($\pm$ 2)

[a] Total electrodeposition charge for Pd, inclusive of H_2 evolution.
[b] Initial resistance in air.
[c] τ_{resp} and τ_{rec} are the response time (R_0 to $0.90R_{max}$, where R_{max} is the steady-state resistance measured at 1000 ppm) and recovery time (R_{max} to $0.10R_{max}$), respectively.
[d] Relative resistance change, $\Delta R/R_0$, observed upon exposure to $[H_2]$ = 1000 ppm in air.

Chapter 4

Conclusion & Perspective

Our research group has been contributing long period efforts in developing H_2 gas sensors since 2001, I have spent most part of my PhD on two generations of these sensors. In 2001, Pd mesowire arrays were invented as the first generation chemiresistive H_2 sensors by taking credits as the state of the art work at that time. Although the mesowires sensors take the advantages of rapid response and recovery behaviors compared with contemporary sensors, the problems of that type of sensors are obvious: The fabrication processes contained electrodeposition on highly oriented pyrolytic graphite (HOPG) electrodes and transferring mesowires on cyanoacrylate films, leading to the shortages of rough precision and low yield. The outstanding methods of lithographically patterned nanowire electrodeposition (LPNE) were invented in 2006, and it has been improved and shared by our group for synthesizing a wide range of nanoscale materials, including metals, semiconductors and polymers etc. In comparison with previously developed HOPG electrodeposition and other synthesis methods, the LPNE method brings the benefits including: (1) Standardized fabrication procedures results in higher yield rate and better quality control, (2) The location, dimension and geometry of nanostructured materials made with LPNE can be well controlled, (3) Complexed structures, for example, core-shell, heterojunctions and nano-ropes, are achievable by

applying LPNE for multiple times. Single pure Pd and Pt nanowire H_2 sensors fabricated with the method of LPNE were invented by our group alumni in 2009 and 2012 respectively, this type of chemiresistive sensors based on single metal nanowires expanded H_2 detection to a new era, benefiting from higher fabrication throughput and yield, enhanced sensitivity and ability to speed up by self Joule heating.

For the purposes of further improvements, single Pd nanowire sensors coated with electrodeposited Pt layers of different thickness were fabricated, characterized and evaluated for the H_2 sensing application. Pt is the noble metal element with higher catalytical activities in dissociating H_2 molecules and producing H_2O than Pd, the reaction rates increase upon the elevated temperature. For the three sets of the Pt thickness, 0.1 monolayer (ML), 1 ML and 10 ML, the optimum Pt loading was 1 ML due to that all key parameters, response, recovery and sensitivity, were accelerated and enhanced.

Until 2015, our group had contributed many efforts in developing H_2 sensors for over 14 years, and successfully pushed the H_2 sensors performance into higher level. During this long period, many changes had been made in sensing parameters and elements, including manipulating the structure, geometry and dimension of the nanowires, combing different metals and applying the Joule heating techniques. It's getting more and more difficult in making improvements after 14 years efforts. The inspiration I had was to amplify the chemical signal from H_2 by further shrinking the critical dimension of sensing element. The ropes of carbon nanotubes (CNTs) own excellent chemical and physical properties to be stable and flexible, making it an outstanding material to serve as transducers for the H_2 sensing application. By partially sharing the experimental procedures of LPNE, the CNTs ropes can be formed by dielectrophoretic deposition, and the surfaces of such CNTs ropes were electrochemically modified by Pd nanoparticles. These Pd@CNTs H_2 sensors exhibited deeply enhanced sensitivity, with a lowest detection limit $\leq$ 10 ppm with respect to 500 ppm from single nanowire sensors, and faster response/ recovery in terms of working at room

temperature.

There is great potential that CNTs ropes can be used in wide applications, not only restricted to detection of H_2. By decorating the CNTs ropes with different materials as sensing elements, such patterned CNTs ropes can be employed for chemical and biological sensing, energy storage, microprocessors, piezoelectric sensors, wearable and portable devices and so forth. This method of lithographically patterned carbon nanotubes dielectrophoretic deposition can be applied on various substrates, including rigid substrates like Si, SiO_2 wafer and glasses, and flexible substrates of polymers and other soft materials. Compared with solid materials nanowires, CNTs are of stronger mechanical and thermal resistance, regarding some extreme working environments.

Bibliography

[1] L. Boon-Brett, J. Bousek, G. Black, P. Moretto, P. Castello, T. Hübert, and U. Banach. Identifying performance gaps in hydrogen safety sensor technology for automotive and stationary applications. *Int. J. Hydrogen Energy*, 35(1):373–384, 2010.

[2] W. Buttner, R. Burgess, C. Rivkin, M. Post, L. Boon-Brett, G. Black, F. Harskamp, and P. Moretto. Inter-laboratory assessment of hydrogen safety sensors performance under anaerobic conditions. *Int. J. Hydrogen Energy*, 37(22):17540–17548, 2012.

[3] W. J. Buttner, M. B. Post, R. Burgess, and C. Rivkin. An overview of hydrogen safety sensors and requirements. *Int. J. Hydrogen Energy*, 36(3):2462–2470, 2011.

[4] M. Carcassi and F. Fineschi. Deflagrations of h 2–air and ch 4–air lean mixtures in a vented multi-compartment environment. *Energy*, 30(8):1439–1451, 2005.

[5] J. Chen, B. Wiley, J. McLellan, Y. Xiong, Z.-Y. Li, and Y. Xia. Optical properties of pd-ag and pt-ag nanoboxes synthesized via galvanic replacement reactions. *Nano Lett.*, 5(10):2058–2062, 2005.

[6] P. Cheng, P. Han, C. Zhao, S. Zhang, X. Zhang, and Y. Chai. Magnesium inference screw supports early graft incorporation with inhibition of graft degradation in anterior cruciate ligament reconstruction. *Scientific reports*, 6, 2016.

[7] B. Choi, D. Lee, J. H. Ahn, J. Yoon, J. Lee, M. Jeon, D. M. Kim, D. H. Kim, I. Park, Y. K. Choi, and S. J. Choi. Investigation of optimal hydrogen sensing performance in semiconducting carbon nanotube network transistors with palladium electrodes. *Appl Phys Lett*, 107(19), 2015.

[8] M. G. Chung, D. H. Kim, D. K. Seo, T. Kim, H. U. Im, H. M. Lee, J. B. Yoo, S. H. Hong, T. J. Kang, and Y. H. Kim. Flexible hydrogen sensors using graphene with palladium nanoparticle decoration. *Sensor Actuat B-Chem*, 169:387–392, 2012.

[9] P. G. Collins, K. Bradley, M. Ishigami, and A. Zettl. Extreme oxygen sensitivity of electronic properties of carbon nanotubes. *Science*, 287(5459):1801–1804, 2000.

[10] S. Dhall, N. Jaggi, and R. Nathawat. Functionalized multiwalled carbon nanotubes based hydrogen gas sensor. *Sensor Actuat a-Phys*, 201:321–327, 2013.

[11] Y. Fan, B. R. Goldsmith, and P. G. Collins. Identifying and counting point defects in carbon nanotubes. *Nature Materials*, 4(12):906–911, 2005.

[12] F. Favier, E. Walter, M. Zach, T. Benter, and R. Penner. Hydrogen sensors and switches from electrodeposited palladium mesowire arrays. *Science*, 293:2227–2231, 2001.

[13] M. Fayette, Y. Liu, D. Bertrand, J. Nutariya, N. Vasiljevic, and N. Dimitrov. From au to pt via surface limited redox replacement of pb upd in one-cell configuration. *Langmuir*, 27(9):5650–5658, 2011.

[14] G. Fisher and J. Gland, JL. The interaction of water with the pt(111) surface. *Surf. Sci.*, 94(2-3):446–455, 1980.

[15] J. Gland, B. Sexton, and G. Fisher. Oxygen interactions with the pt(111) surface. *Surf. Sci.*, 95(2-3):587–602, 1980.

[16] D. Gokcen, S.-E. Bae, and S. R. Brankovic. Stoichiometry of pt submonolayer deposition via surface-limited redox replacement reaction. *J. Electrochem. Soc.*, 157(11):D582–D587, 2010.

[17] S. Grigoriev, P. Millet, and V. Fateev. Evaluation of carbon-supported pt and pd nanoparticles for the hydrogen evolution reaction in pem water electrolysers. *J. Power Sources*, 177(2):281–285, 2008.

[18] S. A. Grigoriev, V. N. Fateev, H. Middleton, and T. O. Saetre. A comparative evaluation of palladium and platinum nanoparticles as catalysts in proton exchange membrane electrochemical cells. *Int. J. Nucl. Hydrogen. Prod. Appl.*, 1(4):343–354, 2008.

[19] S. Gu, X. Wang, Y. Wei, and B. Fang. Mechanism for nucleation and growth of electrochemical deposition of palladium (ii) on a platinum electrode in hydrochloric acid solution. *Sci. China Chem.*, 57(5):755–762, 2014.

[20] G. Gunawardena, G. Hills, I. Montenegro, and B. Scharifker. Electrochemical nucleation: Part i. general considerations. *J. Electroanal. Chem. Interfacial Electrochem.*, 138(2):225–239, 1982.

[21] T. Hübert, L. Boon-Brett, G. Black, and U. Banach. Hydrogen sensors–a review. *Sensor Actuat. B - Chem.*, 157(2):329–352, 2011.

[22] R. C. Hughes and W. K. Schubert. Thin-films of pd/ni alloys for detetion of high hydrogen concentrations. *J. Appl. Phys.*, 71:542–544, 1992.

[23] K. J. Jeon, M. Jeun, E. Lee, J. M. Lee, K.-I. Lee, P. von Allmen, and W. Lee. Finite size effect on hydrogen gas sensing performance in single pd nanowires. *Nanotechnology*, 19(49):495501, Dec. 2008.

[24] K. J. Jeon, J. M. Lee, E. Lee, and W. Lee. Individual pd nanowire hydrogen sensors fabricated by electron-beam lithography. *Nanotechnology*, 20(13):135502, Apr. 2009.

[25] M. Johansson and L. Ekedahl. Hydrogen adsorbed on palladium during water formation studied with palladium membranes. *Appl. Surf. Sci.*, 173(1-2):122–133, Mar. 2001.

[26] G. Kaltenpoth, P. Schnabel, E. Menke, E. Walter, M. Grunze, and R. Penner. Multimode detection of hydrogen gas using palladium-covered silicon mu-channels. *Anal. Chem.*, 75:4756–4765, 2003.

[27] A. Kaniyoor, R. I. Jafri, T. Arockiadoss, and S. Ramaprabhu. Nanostructured pt decorated graphene and multi walled carbon nanotube based room temperature hydrogen gas sensor. *Nanoscale*, 1(3):382–386, 2009.

[28] V. R. Khalap, T. Sheps, A. A. Kane, and P. G. Collins. Hydrogen sensing and sensitivity of palladium-decorated single-walled carbon nanotubes with defects. *Nano Lett.*, 10(3):896–901, 2010.

[29] T. Kiefer, F. Favier, O. Vazquez-Mena, G. Villanueva, and J. Brugger. A single nanotrench in a palladium microwire for hydrogen detection. *Nanotechnology*, 19:125502, 2008.

[30] T. Kiefer, L. Villanueva, F. Fargier, F. Favier, and J. Brugger. Fast and robust hydrogen sensors based on discontinuous palladium films on polyimide, fabricated on a wafer scale. *Nanotechnology*, 21(50):505501, 2010.

[31] G. Korotcenkov, S. D. Han, and J. R. Stetter. Review of electrochemical hydrogen sensors. *Chem. Rev.*, 109(3):1402–1433, 2009.

[32] R. Krupke, F. Hennrich, H. Weber, M. Kappes, and H. v. Löhneysen. Simultaneous deposition of metallic bundles of single-walled carbon nanotubes using ac-dielectrophoresis. *Nano Lett.*, 3(8):1019–1023, 2003.

[33] M. K. Kumar and S. Ramaprabhu. Nanostructured pt functionlized multiwalled carbon nanotube based hydrogen sensor. *J. Phy. Chem. B*, 110(23):11291–11298, 2006.

[34] J. Lee, W. Shim, E. Lee, J.-S. Noh, and W. Lee. Highly mobile palladium thin films on an elastomeric substrate: Nanogap-based hydrogen gas sensors. *Angew. Chem. Int. Ed.*, 123(23):5413–5417, 2011.

[35] J.-H. Lee, W.-S. Kang, C. K. Najeeb, B.-S. Choi, S.-W. Choi, H. J. Lee, S. S. Lee, and J.-H. Kim. A hydrogen gas sensor using single-walled carbon nanotube langmuir–blodgett films decorated with palladium nanoparticles. *Sensors and Actuators B: Chemical*, 188:169–175, 2013.

[36] J. S. Lee, J. Oh, J. Jun, and J. Jang. Wireless hydrogen smart sensor based on pt/graphene-immobilized radio-frequency identification tag. *ACS Nano*, 9(8):7783–7790, 2015.

[37] F. Lewis. Hydrogen in palladium and palladium alloys. *International journal of hydrogen energy*, 21(6):461–464, 1996.

[38] F. A. Lewis. *The Palladium Hydrogen System*. Academic Press, London, 1967.

[39] X. Li, Y. Liu, J. C. Hemminger, and R. M. Penner. Catalytically activated palladiumplatinum nanowires for accelerated hydrogen gas detection. *ACS Nano*, 9(3):3215–3225, 2015.

[40] Y. Lim, Y. Lee, J.-I. Heo, and H. Shin. Highly sensitive hydrogen gas sensor based on a suspended palladium/carbon nanowire fabricated via batch microfabrication processes. *Sensors and Actuators B: Chemical*, 210:218–224, 2015.

[41] T. C. Lin and B. R. Huang. Palladium nanoparticles modified carbon nanotube/nickel composite rods (pd/cnt/ni) for hydrogen sensing. *Sensor Actuat B-Chem*, 162(1):108–113, 2012.

[42] R. Liu, H. Ding, J. Lin, F. Shen, Z. Cui, and T. Zhang. Fabrication of platinum-decorated single-walled carbon nanotube based hydrogen sensors by aerosol jet printing. *Nanotechnology*, 23(50):505301, 2012.

[43] E. J. Menke, M. A. Thompson, C. Xiang, L. C. Yang, and R. M. Penner. Lithographically patterned nanowire electrodeposition. *Nat Mat*, 5(11):914–919, Nov. 2006.

[44] A. Monica, S. Papadakis, R. Osiander, and M. Paranjape. Wafer-level assembly of carbon nanotube networks using dielectrophoresis. *Nanotechnology*, 19(8):085303, 2008.

[45] S. Mubeen, T. Zhang, B. Yoo, M. A. Deshusses, and N. V. Myung. Palladium nanoparticles decorated single-walled carbon nanotube hydrogen sensor. *J Phys Chem C*, 111(17):6321–6327, 2007.

[46] H. Naohara, S. Ye, and K. Uosaki. Electrochemical layer-by-layer growth of palladium on an au (111) electrode surface: Evidence for important role of adsorbed pd complex. *J. Phys. Chem. B*, 102(22):4366–4373, 1998.

[47] J. Nutariya, M. Fayette, N. Dimitrov, and N. Vasiljevic. Growth of pt by surface limited redox replacement of underpotentially deposited hydrogen. *Electrochim. Acta*, 112:813–823, 2013.

[48] T. U. D. of Energy Golden Field Office, editor. *Funding Opportunity Announcement DE-PS36-09GO99004*. Office of Energy Efficiency and Renewable Energy (EERE), 2009.

[49] P. Offermans, H. D. Tong, C. J. M. van Rijn, P. Merken, S. H. Brongersma, and M. Crego-Calama. Ultralow-power hydrogen sensing with single palladium nanowires. *Appl. Phys. Lett.*, 94(22):223110, June 2009.

[50] K. Ogle and J. White. The low-temperature water formation reaction of pt(111) - a static sim and tds study. *Surf. Sci.*, 139(1):43–62, 1984.

[51] M. Palomar-Pardave, I. González, and N. Batina. New insights into evaluation of kinetic parameters for potentiostatic metal deposition with underpotential and overpotential deposition processes. *J. Phys. Chem. B*, 104(15):3545–3555, 2000.

[52] D. Rand and R. Woods. A study of the dissolution of platinum, palladium, rhodium and gold electrodes in 1 m sulphuric acid by cyclic voltammetry. *J. Electroanal. Chem. Interfacial Electrochem.*, 35(1):209–218, 1972.

[53] L. K. Randeniya, P. J. Martin, and A. Bendavid. Detection of hydrogen using multi-walled carbon-nanotube yarns coated with nanocrystalline pd and pd/pt layered structures. *Carbon*, 50(5):1786–1792, 2012.

[54] C. Rivkin, C. Blake, R. Burgess, W. J. Buttner, and M. B. Post. A national set of hydrogen codes and standards for the united states. *Int. J. Hydrogen Energy*, 36(3):2736–2741, 2011.

[55] F. Rumiche, H. H. Wang, and J. E. Indacochea. Development of a fast-response/high-sensitivity double wall carbon nanotube nanostructured hydrogen sensor. *Sensor Actuat B-Chem*, 163(1):97–106, 2012.

[56] P. A. Russo, N. Donato, S. G. Leonardi, S. Baek, D. E. Conte, G. Neri, and N. Pinna. Room-temperature hydrogen sensing with heteronanostructures based on reduced graphene oxide and tin oxide. *Angew Chem Int Edit*, 51(44):11053–11057, 2012.

[57] B. Scharifker and G. Hills. Theoretical and experimental studies of multiple nucleation. *Electrochim. Acta*, 28(7):879–889, 1983.

[58] B. Scharifker and J. Mostany. Three-dimensional nucleation with diffusion controlled growth: Part i. number density of active sites and nucleation rates per site. *J. Electroanal. Chem. Interfacial Electrochem.*, 177(1):13–23, 1984.

[59] S. Shekhar, P. Stokes, and S. I. Khondaker. Ultrahigh density alignment of carbon nanotube arrays by dielectrophoresis. *ACS Nano*, 5(3):1739–1746, 2011.

[60] P. Stokes and S. I. Khondaker. High quality solution processed carbon nanotube transistors assembled by dielectrophoresis. *Applied Physics Letters*, 96(8):083110, 2010.

[61] J. Suehiro, G. Zhou, and M. Hara. Fabrication of a carbon nanotube-based gas sensor using dielectrophoresis and its application for ammonia detection by impedance spectroscopy. *Journal of Physics D: Applied Physics*, 36(21):L109, 2003.

[62] Y. Sun and Y. Xia. Alloying and dealloying processes involved in the preparation of metal nanoshells through a galvanic replacement reaction. *Nano Lett.*, 3(11):1569–1572, 2003.

[63] Y. G. Sun and H. H. Wang. High-performance, flexible hydrogen sensors that use carbon nanotubes decorated with palladium nanoparticles. *Adv Mater*, 19(19):2818–+, 2007.

[64] J. Tracy and P. Palmberg. Structural influences on adsorbate binding energy. i. carbon monoxide on (100) palladium. *The Journal of Chemical Physics*, 51(11):4852–4862, 1969.

[65] R. Vasilic, L. Viyannalage, and N. Dimitrov. Epitaxial growth of ag on au (111) by galvanic displacement of pb and ti monolayers. *J. Electrochem. Soc.*, 153(9):C648–C655, 2006.

[66] E. Walter, F. Favier, and R. Penner. Palladium mesowire arrays for fast hydrogen sensors and hydrogen-actuated switches. *Anal. Chem.*, 74(7):1546–1553, APR 1 2002.

[67] E. Walter, R. Penner, H. Liu, K. Ng, M. Zach, and F. Favier. Sensors from electrodeposited metal nanowires. *Surf. Interface Anal.*, 34(1):409–412, 2002.

[68] J. Wang, B. Singh, J.-H. Park, S. Rathi, I.-y. Lee, S. Maeng, H.-I. Joh, C.-H. Lee, and G.-H. Kim. Dielectrophoresis of graphene oxide nanostructures for hydrogen gas sensor at room temperature. *Sensors and Actuators B: Chemical*, 194:296–302, 2014.

[69] E. Wicke, H. Brodowsky, G. Alefeld, and J. Völkl. Hydrogen in metals ii. *Topics in Applied Physics*, 29:73, 1978.

[70] H. Windhagen, K. Radtke, A. Weizbauer, J. Diekmann, Y. Noll, U. Kreimeyer, R. Schavan, C. Stukenborg-Colsman, and H. Waizy. Biodegradable magnesium-based screw clinically equivalent to titanium screw in hallux valgus surgery: short term results of the first prospective, randomized, controlled clinical pilot study. *Biomedical engineering online*, 12(1):1, 2013.

[71] C. Xiang, S. C. Kung, D. Taggart, F. Yang, M. A. Thompson, A. G. Güell, Y. Yang, and R. M. Penner. Lithographically patterned nanowire electrodeposition: A method for patterning electrically continuous metal nanowires on dielectrics. *ACS Nano*, 2:1939–1949, 2008.

[72] C. Xiang, Y. Yang, and R. M. Penner. Cheating the diffraction limit: Electrodeposited nanowires patterned by photolithography. *Chem. Comm.*, (8):859–873, 2009.

[73] T. Xu, M. Zach, Z. Xiao, D. Rosenmann, U. Welp, W. Kwok, and G. Crabtree. Self-assembled monolayer-enhanced hydrogen sensing with ultrathin palladium films. *Appl. Phys. Lett.*, 86:203104, 1–3, 2005.

[74] F. Yang, K. C. Donavan, S.-C. Kung, and R. M. Penner. The surface scattering-based detection of hydrogen in air using a platinum nanowire. *Nano Lett.*, 12(6):2924–2930, 2012.

[75] F. Yang, S.-C. Kung, M. Cheng, J. C. Hemminger, and R. M. Penner. Smaller is faster and more sensitive: the effect of wire size on the detection of hydrogen by single palladium nanowires. *ACS Nano*, 4(9):5233–5244, 2010.

[76] F. Yang, S.-C. Kung, D. K. Taggart, and R. M. Penner. Hydrogen Sensing with a Single Palladium Nanowire. *Sensor Lett.*, 8(3, Sp. Iss. SI):534–538, JUN 2010.

[77] F. Yang, D. Taggart, and R. Penner. Joule-heating a palladium nanowire sensor for accelerated response and recovery to hydrogen gas. *Small*, 6:1422–1429, 2010.

[78] F. Yang, D. K. Taggart, and R. M. Penner. Fast, sensitive hydrogen gas detection using single palladium nanowires that resist fracture. *Nano Lett.*, 9(5):2177–2182, May 2009.

[79] A. Zangwill. *Physics at Surfaces*. Cambridge University Press, 1988.

[80] X. Zeng, M. Latimer, Z. Xiao, S. Panuganti, U. Welp, W. Kwok, and T. Xu. Hydrogen gas sensing with networks of ultrasmall palladium nanowires formed on filtration membranes. *Nano Lett.*, 11(1):262–268, 2010.

[81] X.-Q. Zeng, Y.-L. Wang, H. Deng, M. L. Latimer, Z.-L. Xiao, J. Pearson, T. Xu, H.-H. Wang, U. Welp, G. W. Crabtree, et al. Networks of ultrasmall pd/cr nanowires as high performance hydrogen sensors. *ACS Nano*, 5(9):7443–7452, 2011.

[82] M. L. Zhang, L. L. Brooks, N. Chartuprayoon, W. Bosze, Y. H. Choa, and N. V. Myung. Palladium/single-walled carbon nanotube back-to-back schottky contact-based hydrogen sensors and their sensing mechanism. *ACS Appl. Mater. Interfaces*, 6(1):319–326, 2014.